J. Water Environ. Nanotechnol., 8(4): 417-441 Autumn 2023

ORIGINAL RESEARCH PAPER

Green synthesis and characterization of Selenium/Zirconium bimetallic nanoparticles using Cinnamomum camphora leaf extract and their photocatalyst and anticancer activity

Mounaguru Sindhudevi[1], Subramanian Srinivasan*[1], Balakrishnan Karthekiyan[1], Arumugam Muthuvel[2,3]

[1] *Department of Chemistry, Annamalai University, Annamalai Nagar, Tamil Nadu, India*
[2] *Department of Physics, Faculty of Science and Technology, Airlangga University, Surabaya, Indonesia*
[3] *Department of Physics, Theivanai Ammal College for Women (Autonomous), Villupuram, Tamil Nadu, India*

Received: 2023-02-07 Accepted: 2023-04-18 Published: 2023-10-19

ABSTRACT
In the present studies, cytotoxicity evaluation of camphor-mediated bimetallic nanoparticles has been done. The IC_{50} values of Te combined Se, Zr, and Ce bimetallic nanoparticles are 18.0, 16.0, 175.4,38.9 µg/ml respectively. A maximum proportion of cell activity attained at 16 µg/ml reveals the size-dependent anticancer property of TeSe, Tezr, and TeCe BNPs towards the MCF -7 Cell line and SeZr towards skin cancer cell lines. The surface morphology with particle size and optical attribute of camphor-mediated BNPs can be analyzed by various studies such as UV- visible spectroscopy, XRD, AFM, SEM –EDX, HR-TEM, and XPS study the size of the SeZr BNPs was observed to less than 100 nm, which conforms to the bioactive nature of bimetallic nanoparticles. In addition, docking activities of some of the components in *camphora extract* (Eugenol, cinnamaldehyde) should be carried out with the breast cancer cell line. In addition, the photocatalytic behavior of *camphor*-mediated SeZr BNPs has been tested by using methylene blue (MB) dye under natural sunlight and UV illumination. The Effect of parameters such as temperature, dye solution at different concentrations, and P^H of the dye solution was evaluated. Hence, the result of the studies shows a maximum of 87% degradation within 60 min for the same concentration solution at P^H 9 which can be due to increases in hydroxyl ion concentration. Further, a comparative study in catalytic activity on photodegradation of MB dye with an optimized sample was carried out under UV irradiation. The reusability test was performed after 60 min degradation, implying the Photocatalyst's stability. Further, a pseudo-first-order kinetic model was performed for the obtained data. This is the first report on catalytic degradation using camphor-mediated SeZr BNPs to effectively remove pollutants in wastewater streams.

Keywords: *Methylene blue, Eugenol, Cinnamaldehyde, Docking activities, Skin cancer cell lines, Breast cancer cell lines.*

How to cite this article
Sindhudevi M., Srinivasan S., Karthekiyan B., Muthuvel A., Green synthesis and characterization of Selenium/Zirconium bimetallic nanoparticles using Cinnamomum camphora leaf extract and their photocatalyst and anticancer activity. J. Water Environ. Nanotechnol., 2023; 8(4): 417-441. DOI: 10.22090/jwent.2023.04.008

INTRODUCTION

The release of textile contaminants from industries to surface water will raise a large variety of environmental challenges. These challenges are creating not only water bodies; Besides, it causes affect aquatic plants and the death of fish and health effects exposure to humans [1]. On the other hand, due to its biodegradable nature, it can affect water at a small concentration of 1PPM (2:3) [2]. Whereases, purification of water from industrial waste is necessary to increase safe and clean water will improve the quality of all life [2]. Therefore, various technologies have been expanding for the removal of contaminants from industrial effluent including filtration, surface complexation, chemical precipitation, ion exchange, membrane processing, flocculation, etc [3]. This way,

* Corresponding Authors Email: *chemssrinivasan@gmail.com*

nanotechnology introduces nanoparticles as a photocatalyst to facilitate the deterioration of organic contamination such as pigment under UV–visible radiation. Seyedehmaryam Moosan et al evaluate photocatalytic activities of synthesized Fe_3O_4/AC/TiO_2 (9:2) through MB dye degradation. The result of these studies presented the highest degradation rate of 98% in 60 min [4]. Further, the photocatalytic evaluation done by Fe_2TiO_5 under natural sunlight shows high degradation capability in a strongly alkaline medium due to increases in the mass of hydroxyl ions [5]. Like, the photocatalytic degradation of MB, this occurs under sunlight irradiation in the presence of cellulose acetate impregnated with ZnO nanoparticles. (CA –ZnO NPs) show more rapid degradation of MB (about 75%) compared to UV–light irradiation (about 30%) at a rate constant of 0.0036 and 0.0114 min^{-1} for UV and sunlight irradiation respectively [6]. The maximum degradation of MB (95%) was achieved in 150 min using 0.015 g of TiO_2 and 0.085g of ZnO (15:85) as a catalyst at P^H 5.9. The green synthesized selenium from an endophytic fungal strain (Penicillium crustose) achieves a degradation efficiency of 84.150% with a subsequent loss of 4% after ten cycles for the degrading of organic dyes [7]. Apart from many photocatalyst usages, Fatemeh Poorsajadvi et al introduce the CuO/Bi_2O_3 nanocomposite for MB dye degradation. hence, the high percent of degradation achieved through this nanocomposite at PH_3 reflects the activities of the photocatalyst in an acidic medium [8]. Further, R. Tayenabee et al tested the degradation efficiency of methylene blue under UV–visible light radiation through a heterogenous photocatalyst of WZNO/HPA. The result shows >40 good activity under sunlight within 90 min [9]. A new and simple method for MB degradation was carried out with AgZnO in visible regions. Occurrence of 98% of degradation using AgZnO and 63% with ZnO [10]. In addition, Elham Parvizi et al have done MB dye degradation using a high-pressure mercury lamp at P^H 9 using MgZnO@SiO_2 tetrazine [11] on the other hand, the presence of heavy metals in the aquatic environment will raise environmental issues as well as create side effects on the living organism in the ecosystem; therefore, reduction of organic compound in pharmaceutical waste and toxic metal such as arsenic, palladium, chromium, has been removed by the nanocatalyst [12]. Along with this, Chuxuan Zhao et al. introduce Fe (III) EDTA complex for degradation of P- arsanilic acid [13] on the basis, Ayoob Rezaein et al fabricate Fe_3O_4@SnO_2/Ag-δGH for the removal of dichlorophenol (93.8%) and a solar visible light induced photodegradation of pentachlorophenol (Mohammad Hossein Sayadi) with Bi/SnO_2/TiO_2 graphene nanocomposite at a rate of 0.001 min^{-1} -0.00149 $min^{-1}$is carried out [14,15]. However, in this way, organic contaminants can deteriorate through condensation and oxidation reactions by converting aromatic alcohols into aldehyde by using commercially available WO_3ZnO/Fe_3O_4, W-ZnO@NH_2-CBB photocatalysts [16,17].

A magnetic photocatalytic nanosystem for toxic drug pollutants has been introduced by Mohammad Hossein Sayadi for the effective degradation of pharmaceutical waste such as gemfibrozil and Tamoxifen (81%), under UV–visible light radiation [18].

Cancer is one of the leading causes of death in the world. According to the 2020 World Cancer Report, approximately 18.1 million new cancer cases and 9.6 million cancer–related deaths are reported every year. As per the WHO survey, in 2020 the global cancer market is expected to reach $150 billion [19]. This may be due to the poor availability of prevention, and diagnosis, as well as inadequate treatment. It is an abnormal or uncontrolled growth of a cell that can proliferate to other healthy tissues of the body. Radiotherapy and chemotherapy are the two pathways utilized for treatment [20]. To overcome such problems in India, recently nanotechnology introduced nanoparticles as anticancer agents for cancer treatment [21]. For this purpose, green synthesis of SeNPs is carried out using a drumstick. it exhibits anticancer consequences against three cancer cells (Caco -2 cells, Hep G2 cells, and MCF – 7 cells). the IC_{50} Value of SeNPs against three cancer cells is 150.87,392.57 and 252.4 µg/ml respectively, indicating dose dependence growth inhibition of three cancer cells [22]. In addition, the Cytotoxicity activity of *Morinda citrifolia*-mediated nanomaterials is tested against HepG2. The result of this study shows high viability at higher concentrations. Hence the Brine shrimp lethality assay shows low cytotoxicity effects, which conforms to the biocompatibility of SeNPs [23]. The antitumor activity of LNCap cancer cells was investigated. The higher the inhibition percentage of SeNPs in cancer cells, which range from 46.3+4.450 to 7.725+11.41 through upregulation of Bax m RNA and downregulated of BCl^{-2} expression,

the better the anti-cancer effect [24]. Further, the comparative treatment of selenium nanoparticles using cell suspension of the protein Acinetobacter SP sw30 and CSeNPs are compared, and the Anti-proliferative activity of SeNPs against 4T1NIH /3T3 Cell and MCF 7 cell is carried out. The result of this study conveys that SeNPs show (20.7%), and (15.8%) more inhibition in cell viability than BSeNPs (53.3%), and (26.6%) respectively [25]. On the other side, CSeNPs (31%) and HEK293 Cells (17%) showed more inhibition in NIH/3T3 cells and HEK293 Cells than BSeNPs (30%) at 100 µg/ml due to strong affinity between positively charged BSeNPs and negatively charged cancer cell surfaces. Finally, the microscopic observation of bacterial cell interaction with SeNPs shows that BSeNPs are a good anticancer agent. Whereases, assessments of BSeNPs on cell migration of 4T1 cells are tested by a wound migration assay. Hence In comparing the activity of SeNPs to that of BSeNPs, the result of this study confirms that bio SeNPs are a better anticancer agent than CSeNPs [25]. In this pathway, apart from single nanomaterials, selenium-decorated TiO_2 can be used to control bacterial infection and prevent the growth of cancerous cells. A high surface charge density of selenium nanoparticles adsorbed on the surface will effectively kill bacteria and cancer cells with no Cytotoxicity effect on non-cancerous cells [26]. Treatment of MCF7 cell lines with different concentrations (25 -100 µg/ml of biosynthesized SeNPs from fenugreek seed extract) exhibit inhibition activity against various pathogenic microorganisms. it shows a high zone of inhibition for Aspergillus niger (12mm), compared to Staphylococcus aureus (8mm) and Escherichia coli (7mm) at different concentrations (10,20,30,40ug/ml) and Cytotoxicity activity of SeNps in the MCF-7 cell lines at 80.83 ug/ml will causes50% death, as confirmed [27]. Anticancer activities of bioactive SeNPs endophytic fungal strain, penicillium crustosum Ep-1, against two cancer cell lines, T47D and HePG2. It reveals a significantly lower value of 95.8+2.9 and 93.4+3.2% in the dark compared to 84.8 +2.9 and 4.6.4+3.3 in the light [7]. The significant decreases in the Ic50 value were obtained at 109+3.8 and 70.4+2.5 against T47D and HePG2 in dark irradiation compared to light irradiation at 19.7+7.2 and 4.8+4.2 ug/ml, which covey the anticancer effect of SeNPs [28], inhibition activities of selenium nanoparticles from the probiotic strain lactobacillus casei ATCC 393 mediated SeNPs will inhibit cancer cell growth and destroy tumor cell by inducing apoptotic cell death and triggering an immune response [29].

The photocatalytic activities of SeZr BNPs are carried out in the current work by degrading organic pollutants such as methylene blue. Hence, the result of these studies revealed that SeZr BNPs is a promising photocatalyst for the effective removal of MB dye contaminants under visible light irradiation, suggesting that it is a suitable material for the removal of contaminants from wastewater Strems. However, the present study aimed to use bio-fabricated *camphora* mediated SeZr BNPs to overcome the major issue that arises in environmental crisis as well as in cancer treatment. In addition, a cytotoxicity evaluation of *camphora* - mediated bioactive BNPs was done. A TeSe BNPs in 1:1 concentration is issued for anticancer prediction. The bimetallic nanoparticles at above 300 µg/ml show promising anticancer activities in opposition to MCF -7 cell lines, a kind of breast cancer cell. The IC_{50} value of camphor–mediated Te combined with Se, Ce, and Zr nanoparticles will show that nanoparticles should have the potential to diagnose an infection arising from cancer protein. An experimental and theoretical determination carried out with the MCF -7 Cell line suggests the SeZr BNPs are suitable materials for cancer treatment.

EXPERIMENTAL METHOD

Materials

All the chemical substances used in the method were A.R Grade and obtained from the Sigma Aldrich branch, India. Filtration was done by using What Man 40 filter paper. Chemicals such as sodium selenite (10102-18-8), and Zirconyl chloride (7699-43-6), were purchased from the Subra Scientific store in Pondicherry, India. Methanol (26-67-56-1) was bought from S. Devi Chand & Co (chem.) Private Limited. Chennai, India. Further, the chemicals methylene blue (61-73-4) sodium hydroxide (CAS:1310-73-2), and hydrochloric acid (CAS:7647-01-0) were purchased from Nice Chemicals Pvt. Ltd Cochin, India.

Preparation of leaf extract

Initially, about 30g of the finely powdered leaf (*Cinnamomum Camphora)* was weighed. The extracting solvent (Methanol) in a 1:10 ratio was added to a conical flask. It was stirred for about 30 min at 64 °C. As a result, the methanol-soluble components in plant products were removed.

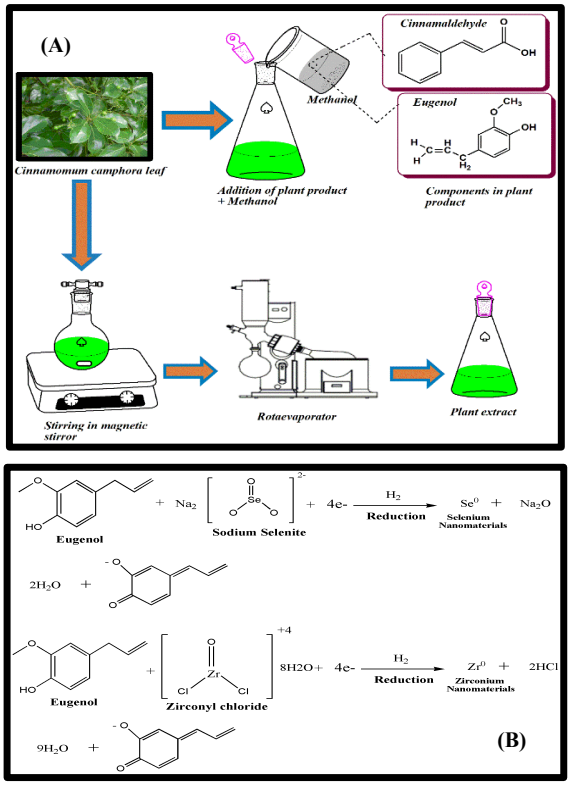

Fig. 1:(A) Scheme of plant extract preparation method ; (B) Scheme diagram of synthesis method of bimetallic nanoparticles

Further, junk content was removed by the filtration process. The filtrate obtained was subjected to a rotary evaporation process for solvent separation. Finally, plant extract acquired from the rotary evaporation process was utilized as reducers in biosynthesis.

Synthesis of nanomaterials

It is carried out by using a 0.0001M solution of sodium selenite and Zirconium chloride (Fig. 1). An equal molar proportion of metal solution is pipetted into a conical flask, and 40 ml of plant extract is added in a 1;4 ratio to the reaction mixture. Then it was stirred with a magnetic stirrer for 6h. The color change from colorless to brown indicates the formation of Sezr bimetallic nanomaterials.

Anticancer activities

Cell viability assay, HCT116 viable cells were harvested and counted using a hemocytometer, diluted in DMEM medium to a density of 1×10^4 cells/ml, seeded in 96 well plates for each well, and incubated for 24 h to allow attachment. After HCT116 cells were treated with the control, a solution containing different concentrations (10 - 70 µg/ml) of aqueous extracts was applied to each well. HCT116 cells were incubated at 37°C in a humidified 95% air and 5% CO_2 incubator for 24 h. After incubation, the drug-containing cells were washed with fresh culture medium, and the MTT (5 mg/ml in PBS) dye was added to each well, followed by incubation for another 4 h at 37°C. The purple precipitated formazan that formed was dissolved in 100 µl of concentrated DMSO, and the cell viability was measured by absorbance at 540 nm using a multi-well plate reader. The results were expressed as the percentage of stable cells concerning the control. The half-maximal inhibitory concentration (IC_{50}) values were calculated, and the optimum doses were analyzed at different periods.

$$\text{Inhibitory of cell proliferation (\%)} = \frac{\text{The mean absorbance of the control absorbance of the sample}}{\text{The mean absorbance of the control}} \text{ X } 10$$

The IC_{50} values were determined from the aqueous extract's dose-responsive curve, which showed 50% inhibition of cytotoxicity compared to control cells. All investigations were conducted at least three times in triplicate.

Molecular Docking Activities

The information about the compound Eugenol, Cinnamaldehyde related to docking activities is collected from the literature, and the structure of the ligand that was needed for docking is drawn using the chem draw 8.0 software. A Selection of suitable anticancer receptors and their structure were downloaded from a protein data bank.

Evaluation of photocatalytic activities

The photocatalytic action of the synthesized SeZr BNPs was evaluated using a 0.00001M solution of methylene blue at three different PH levels under visible light radiation. In this experiment, 50 mL of a 0.00001M dye solution was pipetted into a degradation tube and labeled O'. The photocatalyst was mixed with a dye solution and ultrasonically sonicated for 15 min to obtain a uniform dispersion of NPS. The concoction was stirred in a magnetic stirrer in the dark for 30 minutes to attain adsorption-desorption equilibrium between the dye solution and catalyst. Then 5 mL aliquots were withdrawn into different measuring jars every 10 minutes. The concentration of the test solution after light illumination (5 mL) was determined by using (UV - Shimadzu 2450 Spectrophotometer) at 200-800 nm wavelengths, respectively. A similar protocol was repeated for different pH solutions.

CHARACTERIZATION

UV–visible spectroscopy

UV-visible spectroscopy has been proven to be a very appropriate, systematic, and quite sensitive tool for preliminary confirmation of nanoparticles. The reduction of K_2TeO_3 and Na_2SeO_3 metal precursors was monitored by measuring the UV-visible spectrum of the reaction mixture over a range of 200 -800 at different time intervals (Shimadzu UV -1650 pc Spectrophotometer, Japan, East Asia) at a resolution of 0.5nm. The UV - spectra were noted in an optical glass cuvette of 1cm light path length and concerning Deionized water. The experiment was performed at room temperature. it was prepared by dissolving a sample in a 100Ml volumetric flask using a solvent (methanol).

UV –diffuse reflectance spectroscopy

UV – DRS Spectra of Biosynthesized TeSe BNps were recorded using a (UV -3600 Shimadzu Spectrometer Japan East Asia) and $BaSO_4$ as a Standard at 800 -200nm. The bandgap of BNPs for tellurium in combination with selenium at different concentrations has been determined on the Tauc plot. The plot of $F(R)*(hv)^2$ versus hv (eV) proves the indirect (Te) and direct (Se) bandgap of the synthesized nanomaterial. The sample was prepared for Synthesized BNPs by pilling a small amount on a layer of barium sulfate powder, after which the powder was spread into a thin, uniform layer using a glass rod suitable for band gap prediction.

XRD

XRD diffraction spectra were recorded on the Shimadzu XRD 6000 (Europe, India). The X-ray Diffractometer system operated at a voltage of 40Kv and a current of 30mA with Cukα radiation in Θ - 2Θconfiguration in the scan range 5.0-8.0. The X-ray intensities have been noted from 10-80 and 2Θ angles. In XRD analysis, a needed quality of talc-like powder was obtained by grinding a freeze-dried sample using a mortar and pestle.

SEM – EDX

The surface morphology and size of the purified TeSe BNPs were studied with scanning electron microscopy (SUPRA55 –CAROZEISS, Germany, India) operating at 20kv. Energy dispersive spectroscopy analysis was conducted with the same instrument for constituent analysis of the sample. In SEM analysis, sample preparation of nanopowders or particles was carried out by taking a small amount of sample with a spoon and placing it in a carbon double-side sticker, then using a sprayer to remove the excess particles

DLS

The particle size measurement of biosynthesized BNPs from 0.3mm diameter to 5 microns is carried out using 90° degree scattering optics. The zeta potential of colloids and nanoparticles is done on patented M3 –PALS technology in New Delhi, India using He –Ne Laser at 633 nm using 10mv. The temperature range extension option to 120°c. the sample solution was prepared by dissolving an appropriate amount of sample in 20Ml of liquid or 1:1000 dilution must be sufficient for particle size analysis.

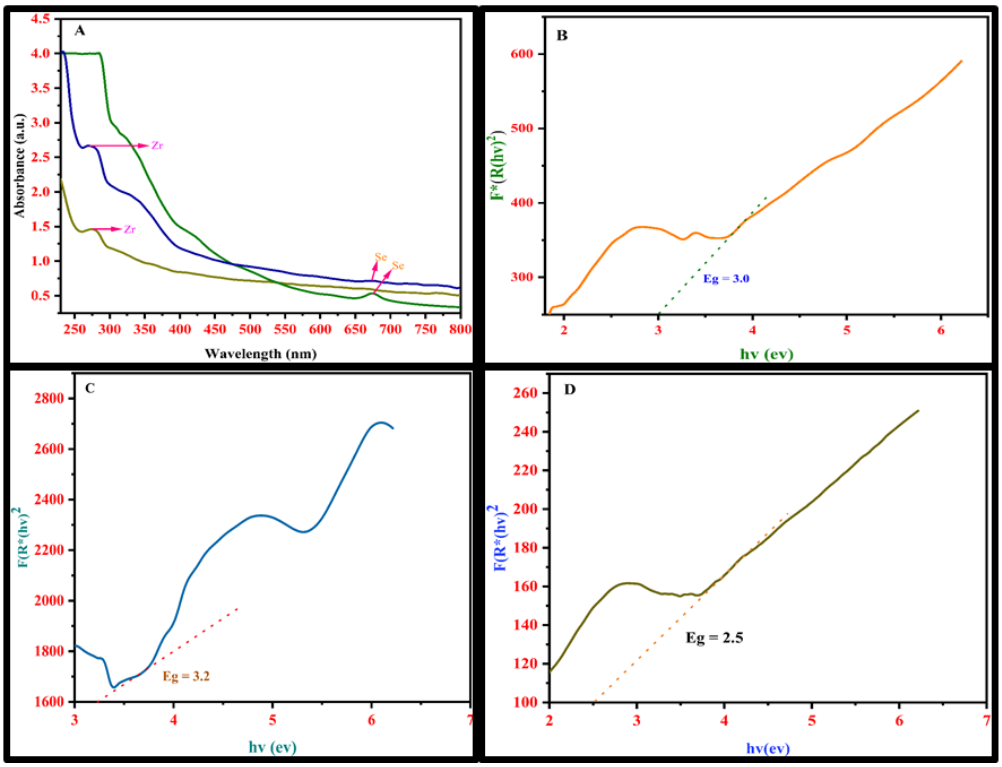

Fig. 2:(A) UV - visible spectrum of *C. Camphora* leaf extract mediated monometallic Se, Zr with SeZr BNPs (B-D) UV diffuse reflectance spectrum of SeNPs, ZrNPs and SeZr BNPs

HR-TEM

Surface morphology and Size of BNPs were analyzed by HR – TEM using an FEI Techai G2 2505 –Twin at 200kv, Maharastra India, using LeB6 or W emitter. It operated with 25X – 1030Kx magnification. it was prepared by dissolving a suitable amount of powdered sample in a particular solvent and by deep coating carbon on the filmed grid in the solution and leaving the grid to evaporate the solvent for hours before analysis.

AFM

AFM microscopy Park N x10 S1CM Korea, India was applied to observe the morphology and surface topography of the BNps using tapping mode with RTESP tip. The resonance frequency of the tip was 281.33 kHz and the scanning range was 2.0 µm. The sample was prepared by mixing a suspension in ethanol or water with 0.1mg/ml concentration.

XPS

XPS measurements were performed with (Thermo Fisher scientific K -Alpha) XM1000 Bangalore, India, monochromator model x-ray photoelectron spectrometer with Al -Kα radiation of 1483 Ev operated at 300 W (20mAemission current,15Kv) and a base pressure of 5x10-5m bar. Sample preparation was carried out by dissolving the powder in a suitable solvent and then drop cast onto the surface of a clean silicon wafer for elemental analysis.

RESULT AND DISCUSSION

UV–visible spectroscopy

The visible attributes of Biosynthesized SeZr BNPs have been described by their UV–-spectroscopy. UV–visible spectrum of bioactive SeZr BNPs is illustrated below in Fig 2. The adsorption peak of selenium is absorbed at 670nm and that of zirconium at 275 nm, indicating the surface Plasmon resonance peak of colloidal SeZr BNPs [31]. A formation of two separate peaks in two distinct regions conforms to the non-–aggregate form of the spherical shape SeZr BNPs. A shift in the absorption band at nearly 600 -700nm suggests that synthesized nanoparticles were relatively small. The energy gap of SeZr BNPs is predicted

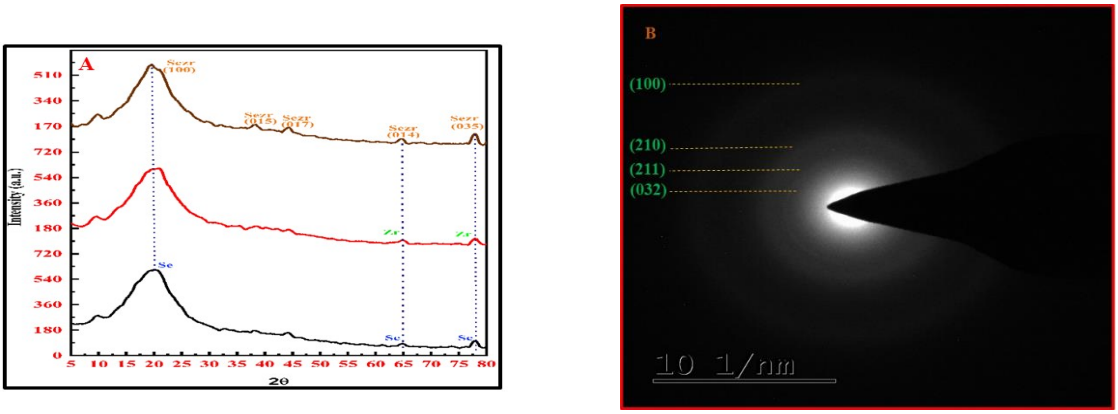

Fig. 3:(A) XRD spectrum of *C. Camphora* leaf extract mediated monometallic Se, Zr with SeZr BNPs (B) SAED pattern of biosynthesized SeZr BNPs

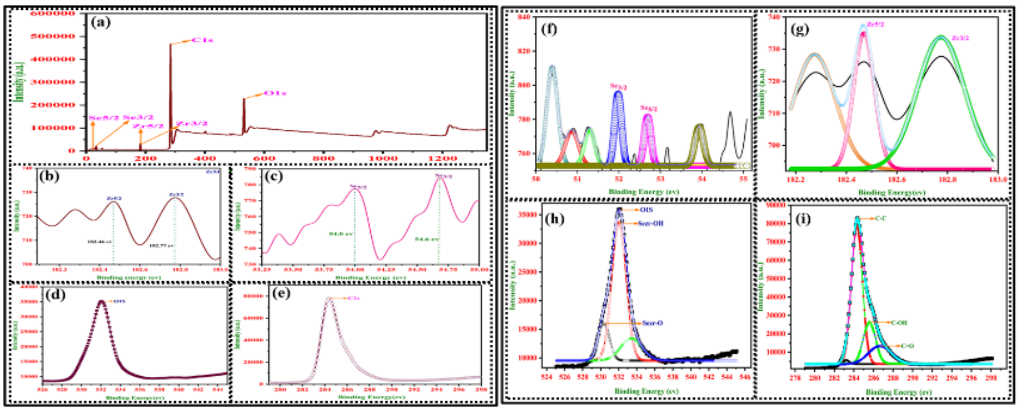

Fig. 4:(A) Xps spectrum of camphora – mediated SeZr BNPs (B)Se (C) Zr (D) O1s (E) C1s (F)Deconvolution spectrum of Se (G) ZrBNps(H) O1s (I) C1s

using Tau's equation. Fig 2. (b) Ultraviolet violet diffuse reflectance spectroscopy of SeZr BNPs and monometallic Se. The band gap of BNPs is 3.1 eV, which corresponds to particles having a mean diameter of 101.6±9.8 similar to previously reported literature [32]. The increases in band gap for Se from 2.5 to 3.0 on combining Zr with Se indicates that camphor-mediated SeZr BNPs have been a suitable material for photocatalytic activity.

$$\xi hv = C\,(hv - Eg)^2 \qquad (2)$$

where ξ - adsorption coefficient
hv – the energy of the incident photons

XRD

XRD spectrum of hexagonal phase SeZr BNPs is given below in Fig 3. was compared with JCPDS card no:86 -2246 and 89 -2340. The hexagonal phase of SeZr BNPs in planes (100), (210), (211), and (032) conforms to the amorphous SeZr BNPs. A formation of a bulk peak will show the amorphous nature of SeZr BNPs. A broad diffraction peak was observed at the (100) plane of amorphous SeZr BNPs. The remaining peak at three distinct regions (210), (211), and (032) conforms to the individual plane of Se and Zr nanomaterials. Hence, it is mentioned that the combination of se with Zr does not influence the phase of BNPs [33]. In addition to XRD analysis, the SAED pattern conforms to the amorphous nature of nanomaterials [34].

SEM –EDX:

An SEM image of SeZr BNps illustrates the grain size distribution of nanomaterials (Fig. 4). It was observed that the grain size of SeZr BNPs is smaller and has shrunk a little bit due to the drying process. Energy dispersive X-ray spectroscopy was

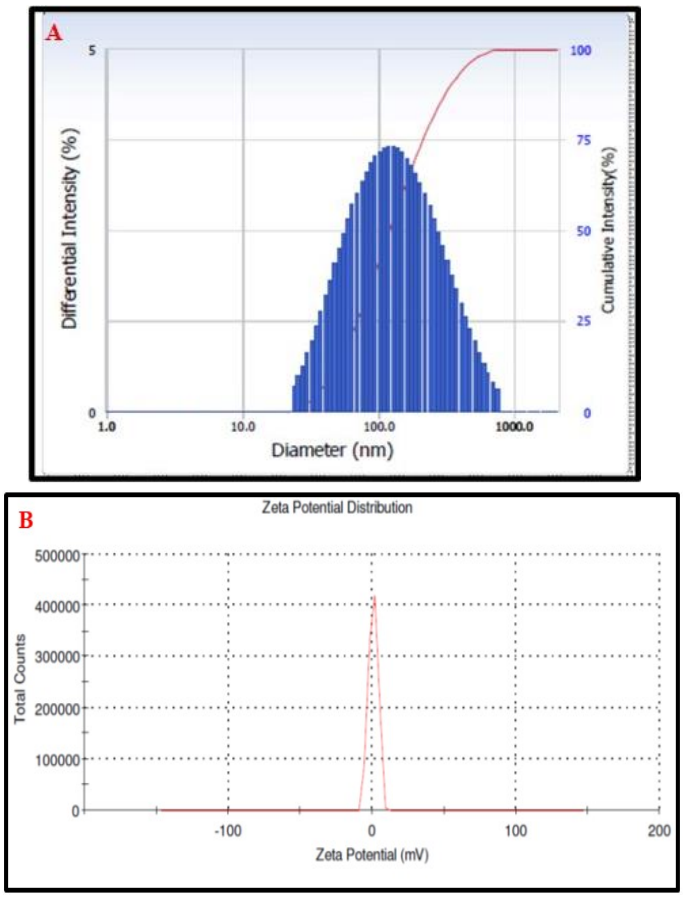

Fig. 5:(A)The hydrodynamic diameter (B) zeta potential of camphora-mediated SeZr BNPs

used to analyze the elemental composition of SeZr bimetallic nanomaterials. The signal could appear at above 30,000 intensity counts in the range of 0-5, confirming the presence of SeZr BNPs. The atomic ratio of SeZr BNPs reveals the percentage of metal nanoparticles. A lack of some other peak with a high amount of Se peaks confirms the purity of the nanomaterials [35, 36].

DLS:

The granular size distribution of SeZr BNPs is measured by dynamic light scattering. The mean of SeZr BNPs is in the range 100 – 170 SD 39.0 with a PDI value of 0.3, which conforms to the dispersive nature of SeZr BNPs in deionized water (Fig. 5). The result of studies has been similar to a TEM analysis and previously reported literature [25, 36, 37].

XPS:

An XPS analysis of BNPs showed the characteristic of C1s and O1s interior level peaks for SeZr BNPs (Fig. 6). Further, the deconvolution spectra of bimetallic nanoparticles in Gaussian components reveal the characteristic of BNPs. The deconvolution spectrum of Zr, Se consists of two peaks at 54.0,54.6 corresponding to Se2p3/2 and Se3d5/2 of SeZr from the Xps database, the result indicates that Se, Zr in SeZr BNPs will exist as Se (0) oxidation in combination state. The survey spectra of XPS for *camphora*-mediated Bioactive SeZr BNPs and their element concentration at the surface are listed in Table 1. The binding energies of Se, Zr, O, and C in the sample were 34.0,34.6,182.46,182.77,35000, respectively. The result of this study coincides with the EDX report. A formation of two sharp peaks at 34.0,34.6 eV shows a similar report compared to the literature report that could assign the binding energy of se, Zr as se2p3/2, Se2p1/2, $Zr2p_{3/2}$, $Zr2p_{1/2}$ respectively. This conforms to the Se^{2+} in the SeZr BNPs as a photocatalyst [38,39].

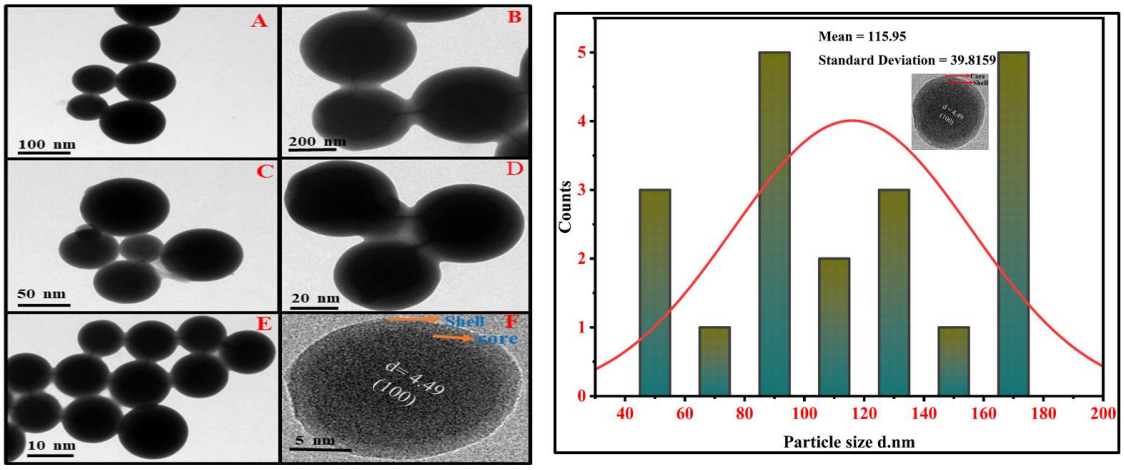

Fig. 6:(A) HR-TEM images *C. Camphora* leaf extract mediated SeZr BNPs (B) Particle size distribution of *C. Camphora* leaf extract mediated SeZr BNPs.

Table 1. illustrates the binding energy and FWHM value of elements C_{1S}, O_{1S}, Se_{3d}, Zr_{3d}

S.No	Name	Binding Energy	FWHM	Area(p)cps ev
1	C_{1s}	284.39	1.74	180598.83
2	O_{1s}	532.04	2.29	75104.93
3	Se_{3d}	62.2	62.38	461.1447
4	Zr_{3d}	182.4	6.88	409.88772

Table 2. Surface area with a surface roughness of SeZr BNPs

S.No	Nanomaterials	Surface area(μm^2)	Surface roughness(nm)	Root mean square(nm)
1	Sezr	4391	4.4655	6.38077
2		8712	3.65765	5.6441
3		8779	3.78036	5.19195

HR –TEM

The surface morphology of *Cinnamomum camphora*-mediated SeZr BNPs was studied. The spherical shape SeZr in uniform distribution is shown in Fig. 7. The average particle size of SeZr BNPs is between 100 -170 nm, similar to DLS, AFM study. Similar to SeZr BNPs, much of the previously reported literature shows selenium synthesis by some bacteria and plant species, such as bacterial strain JS -11 and Klebsiella pneumonia. Hence, the larger size of the nanomaterials is due to the aggregation of particles. present studies confirm the capping ability of bioactive components in *camphora* extract [40].

AFM

Surface topography and structural analysis of bioactive SeZr BNPs are carried out by AFM study. It reveals the nanoparticles are spherical with aggregation and are in the Nano size range. The surface topography of 2D and 3D dimensional SeZr BNPs is shown in Fig. 8. The 2D image shows the aggregate form of SeZr BNPs, with an average particle size of SeZr BNPs in the range of 45 – 90 nm. Whereases, a 3D image visualized the surface roughness of BNPs at a maximum height of about 0 -90 nm in the Z direction. The surface roughness of SeZr BNPs is 4.6554, 3.78036, and 3.65765nm at three distinct regions, respectively (Table. 2). The exterior area of SeZr BNPs (8779, 8712, 4391μm^2) increases with increases in surface roughness suggesting that SeZr BNPs be a suitable material for catalytic activity [41].

Anticancer Activities of ZrSeBNPs

In vitro, Cytotoxicity estimation of *camphorea-*

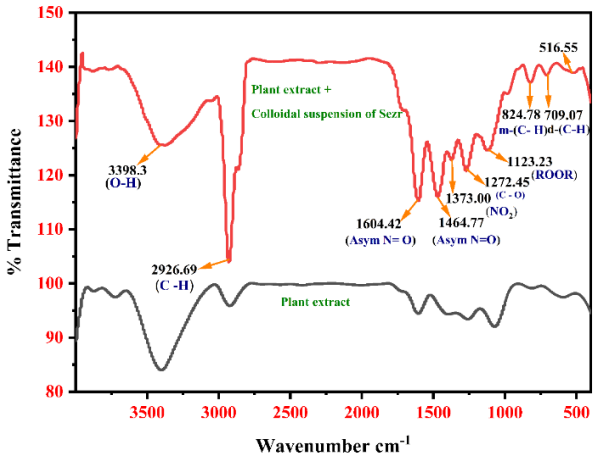

Fig. 7: FTI-R spectrum of (A) *C. Camphora* leaf extract (B) *C. Camphora* leaf extract mediated SeZr BNPs

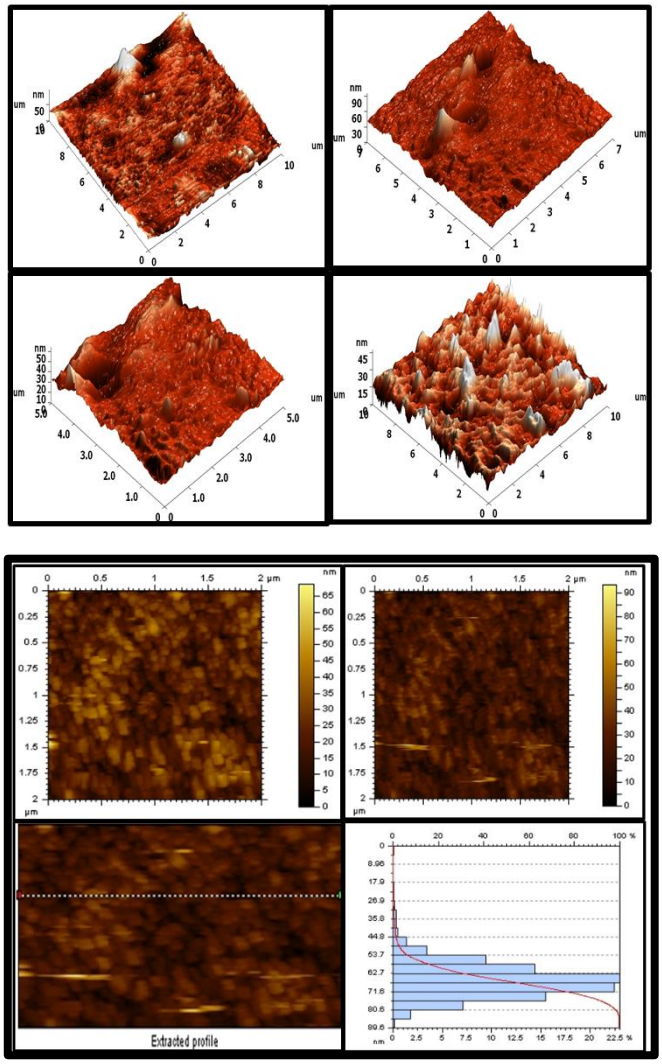

Fig. 8. 2D and 3D topography of Cinnamomum camphora mediated by SeZr BNPs

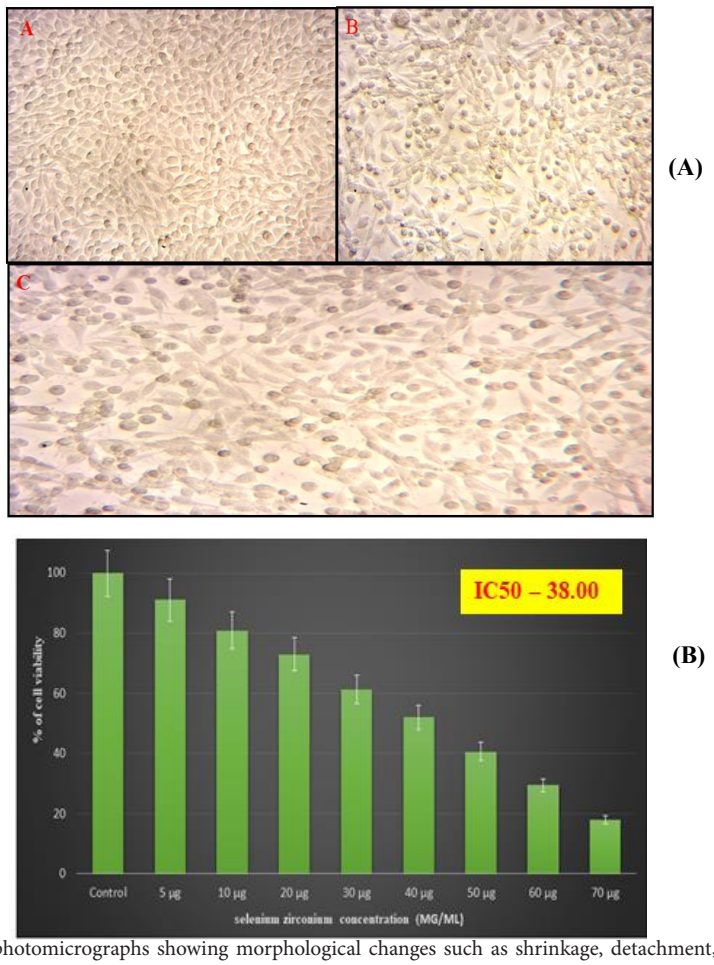

Fig. 9:(A) Representative photomicrographs showing morphological changes such as shrinkage, detachment, membrane blebbing, and distorted shape in the SK-MEL-3 cancer cell lines treated with selenium zirconium; (B) Anticancer consequences of selenium zirconium on the activity of immunosuppressive in skin cancer cells

mediated Zr-Se BNPs at various concentration ranges (5 – 30 µg/ml) was performed with the MCF -7 cell line (breast cancer cell line) for 24h by MTT assay. Experimentation with MCF -7 cells shows decreases in cell viability with increases in BNP concentration for all systems, even at constant cell proliferation after 24 hr of growth. The Retainment of cytocompatibility within BNPs (cell growth greater than 60%) for concentrations up to 15 µg/ml will be experimentally predicted. While depletion of cell proliferation was found at concentrations higher than 25µg/ml for BNPs [42]. The IC_{50} value of ZrSe BNPs in the range of 18.5 is higher than Bio –SeNPs from Drum Strick and Actinobacteria Sp SW30 showing the proliferative effect of BNPs [25]. SeNPs have a lower inhibition potential against prostate cancer line (46±4.4% to 77.2± 11.4) at 4-6 µg/ml concentration than BNPs, demonstrating the synergistic and cytocompatibility properties of nanomaterials. Finally, the appropriate toxicity of bacterial cells and the irrelevant Cytotoxicity to non-cancer cells intimate the arrival of ZrSe BNPs as a future antimicrobial drug. However, future drastic and persistent studies using animal mode should be carried out to confirm ZrSe BNPs as a viable drug.

Photomicrograph represents deformation changes in MCF -7 lines such as abatement, dissolution, membrane blebbing, and distorted shape activated by TS treatment (15 and 20 µg/ml for 24 h) in contrast with control. Control cells showed normal unaltered cell cytology and their images were recorded by a light microscope.

The MCF-7 cells were processed with various concentrations of TS(5-30 µg/ml) for 24 h and the results are expressed as a % of the control value in presenting a cell cytotoxicity ratio for MCF-7 cells using the MTT assay. Data were presented as mean

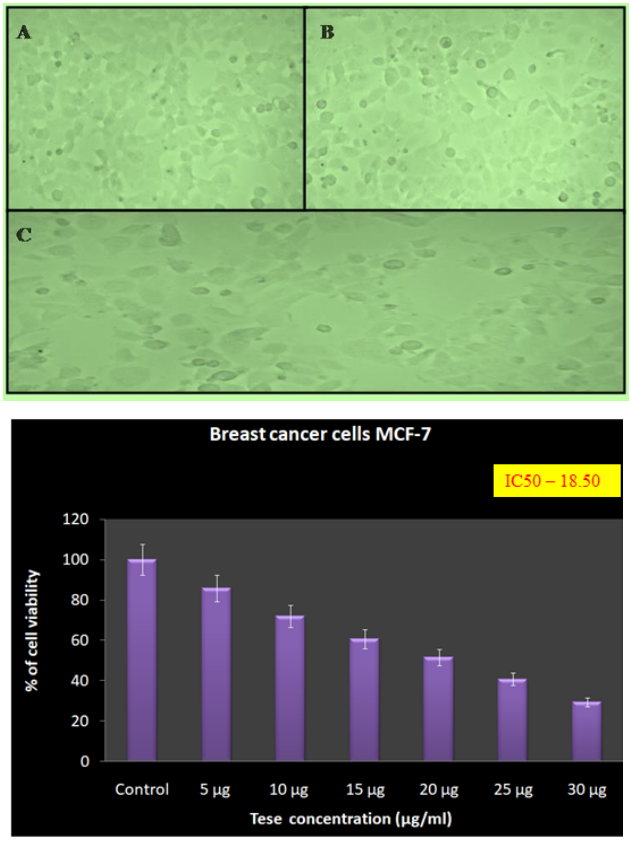

Fig. 10:(A) Illustrate the photographic image of MCF -7 treated with TS at noon ; (B) Anti-cancer effects of TS on the activity of cytotoxicity in breast cancer cells MCF-7.

F10

± SD asterisks, indicating statistically different experiments compared to the control (Fig. 9).

Anticancer Activity *OF TeZr* BNPs

Cytotoxicity activity of Tezr BNps from Camphora – Mediated Bioactive Nanoparticles has been assessed by MTT assay compared with control. The maximum level of cell inhibition attained at 15ug/ml is lower than previously reported literature showing the Cytotoxic behavior of BNPs [43]. The IC50 value of Camphora mediated Tezr BNps is 16.50, respectively. The outcome of this study is confirmed by cell membrane destruction. Anti-proliferative effect of TeZr on the activity of Cytotoxicity in breast cancer cells (MCF -7 Cells). Fig. 10 illustrates the proportion of cell proliferation at different concentrations. A higher Inhibitory potential for TeZr BNPs than Monometallic compounds confirms the synergistic effect of BNPs. The synergistic effect of BNPs can be estimated using the formula.

(B-A/A) x 100

A comparison of the anticancer effect of tellurium containing some fewer toxic metals Zirconium, Cerium, and Selenium) reveals a lower IC_{50} (16.50) than other metals due to its small size, which will favor surface charge interaction on the surface and lead to ROS generation, which will induce bacterial growth inhibition.

The breast cancer cells were processed with various concentrations of TZ (5-30 µg/ml) for 24 h and the results are expressed as a % of the control value in presenting a cell cytotoxicity ratio for MCF-7 cells using the MTT assay. The statistics were displayed as mean ± SD asterisks indicating statically different experiments compared to the control (Fig. 10 (b)).

Anticancer activities of TeCe Bimetallic Nanoparticles

A cytotoxicity evaluation of CeO_2 against cancer cells is done using the MTT assay. Incubation of the MCF -7 cell line with TeCe for 24 hours leads to

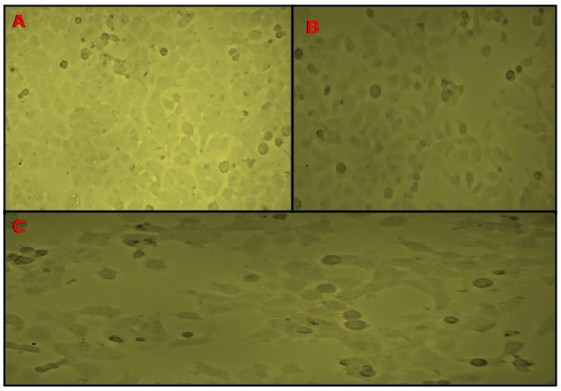

(A)

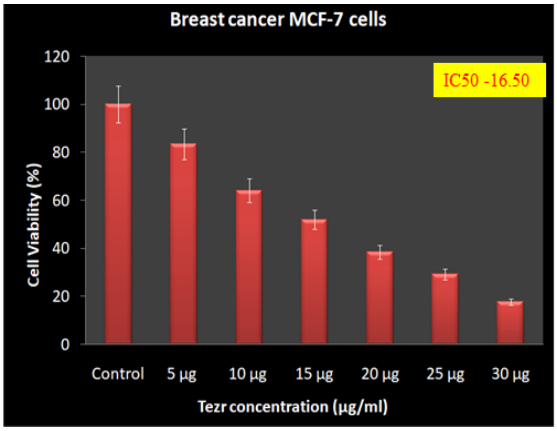

(B)

Fig. 11:(A) Representative photomicrographs of breast cancer cells treated with TZ at 24 h; (B) Anti-cancer effects of TZ on the activity of cytotoxicity in breast cancer cells MCF-7.

cell discharging and shrinking. A MIC (minimum inhibitory concentration) needed for inhibition activities (IC50 -175.4ug/ml) is similar to calcinated cerium oxide (M. Sridharan et al) [44]. A Maximum decrease in cell viability of about 80% at MIC 500mg/ml from bioactive Origanum Majorana L.leaf extract [45]. Artocarpus gomezianus fruit extract mediated Nano ceria (IC50 -479.56µG/ML) confirms the inhibition action of BNPs [46]. Further, a lack of half-lethal killing effect (50%) was noticed at 31.2µg/ml for the CeO_2/ZnO nanocomposites and 62.5µg/ml for ZnO NPs, and 100µg/ml will induce 56% of cancer cell death through silver/gold loaded cerium oxide nanoparticles [47] is less potent than BNPs, which is consistent with the inhibition action of BNPs. Finally, in some of the recent studies, hybrid Nano ceria from sol-gel synthesis and *Nelumbonucifera gaerlin* flower, encapsulated CeO_2 NPs (IC50 -41.60µg/ml,0.20±0.01µg/ml, Swathi pons-8.09±1.55µg/ml) be lessor than TeSe BNPs shows the biocompatibility of BNPs [48,49]. Observation of the antiproliferative effect of hybrid biomaterials cerium –Amino clay against HCT116 cancer cells at high conc 15mg/ml will exhibit impressive antitumor efficiency than the TeSe BNPs and prove biocompatible [50].

Photomicrograph (40x) represents morphological changes in HCT116 cells such as shrinkage, detachment, membrane blebbing, and distorted shape induced by black tea treatment (100 and 150 µg/ml for 24 h) as compared with control. The Control cells showed normal intact cell morphology and their images were captured by a light microscope.

The **MCF-7.** cells were treated with an increasing concentration of TC(25-300 µg/ml) for 24 h and the results are expressed as a percentage of the control value in presenting as a cell cytotoxicity ratio for **MCF-7** cells using the MTT assay. Data were presented as mean ± SD asterisks, indicating statistically different experiments compared to the control (Figs. 11 & 12).

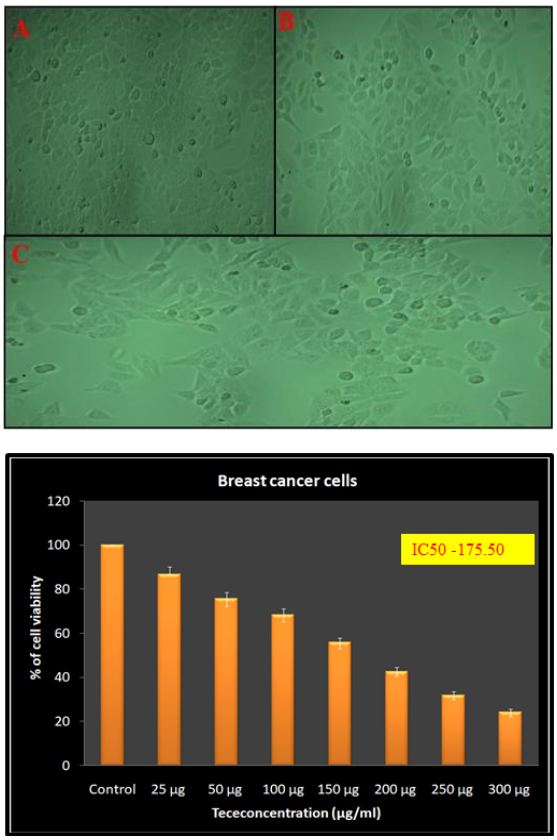

Fig. 12:(A) Morphological changes in control and black tea treated colorectal cancer HCT116 cells for 24 h; (B) Effect of TC on the cell viability of human Breast cancer MCF-7 cells were assessed by MTT assay.

Anticancer activities of SeZr BNps

The anticancer activity of SeZr BNps is tested against skin cancer cell lines at six different concentrations (5 -70µg/ml) by MTT assay (Fig. 13). The minimum inhibition concentration of camphora-mediated SeZr BNps is 38.00µg/ml for cell lysis. IC50 value of SeZr BNps is 38.00µg/ml. The percentage of inhibition was increased with increases in the concentration of SeZr BNps revealing the inhibition potential of Bimetallic nanoparticles towards lower concentration. The report of this study is best compared to previously reported literature, Zr-doped ZnO, thin Nano plates against MDA-MB-231 cancer cell lines [51]. The effect of bilirubin on HDF, A431, and SKMEL -3 cells was 125,115 and 95µM at 24 hr and 115,100, and 75µM at 48 hr respectively will induce apoptosis in SK MEZ -3 and A431 cancer cells are more than normal HDF cells.[52] The cell activity of U -87 cell lines after treating them with nanocomposite hydrogels at a concentration of 100mg/ml for different time intervals (24, 48 & 72 hr) will be focused on the apoptotic response of nanocomposite hydrogels against U-87 cell lines. [53]Further, the anticancer consequences of Nps (Zr –MOF@ppa@PEG) Nps against mouse breast cancer 4T1 cell lines will undergo 90% inhibition is lesser than camphora – mediated SeZr BNPs (5µg/ml) revealing the cytotoxicity of SeZr BNPs [54]. Cell viability of SeZr BNPs is lesser than standard drug (control) and inhibition activities of human breast cancer and human fibroblast cell line at low concentration100µg/ml by MTT assay using zirconium phosphate reveals the biocompatibility of SeZr BNPs. Further, a comparative study on the anticancer effect for *camphora*-mediated BNPs will reveal higher activities towards catalyst in the order of TeSe, TeZr, SeZr thanTeCe BNPs due to variation in size distribution conforms to the activity of photocatalyst.

Anti-cancer result of selenium zirconium on the action of chemotherapeutic SK-MEL-3 cells. The cells were refined with an increasing concentration of selenium zirconium (5-70 µg/ml) for 24 h and the results are expressed as a percentage of the

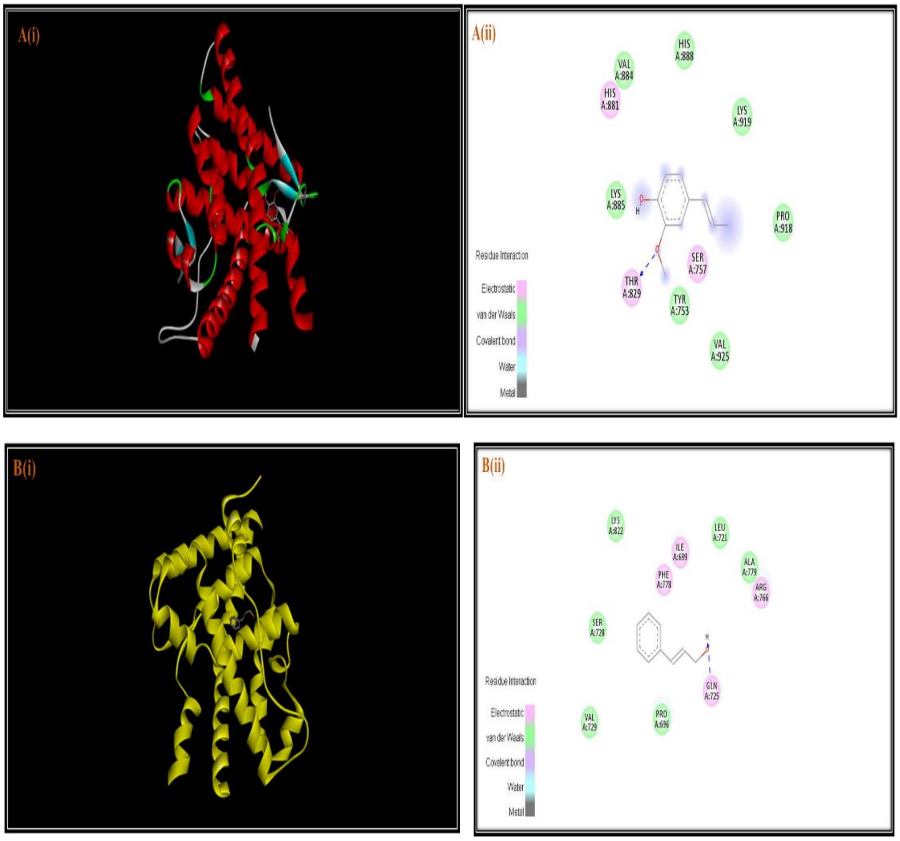

Fig. 13:(Ai -Bii) 2D and (Aii-Bii) 3D image of compound (*Eugenol, Cinnamaldehyde*) with cancer protein

Table 3. Illustrate the statistical data for camphora-mediated bimetallic nanoparticles

S.No	Nanomaterials	Mean	Median	Standard deviation
1	Tese	17.5	17.5	9.3541
2	Tezr	17.5	17.5	9.3541
3	Sezr	35.625	35	23.5186
4	Tece	153.57	150	102.4985

control value in presenting as a cell cytotoxicity ratio for SK-MEL-3 cells using MTT assay. The statistical analysis for the percentage of cell viability reveals a mean and standard deviation for bioactive photocatalysts. Table 3. illustrates the statistical data for camphora mediated bimetallic nanoparticles.

Evaluation of photocatalytic activity:

The photodegradation of methylene blue under a UV source was taken as an observatory tool to study the photocatalytic performance of synthesized SeZr BNps. Fig. 14 (A) UV spectrum of MB dye after light illumination. The photocatalytic activities of bioactive camphor-mediated SeZr BNps are evaluated by degrading methylene blue dye. The UV-visible spectrum of methylene blue with SeZr catalyst after light illumination has been shown in Fig. 14 (B). The experiment was accomplished in the Herber photo reactor's UV light irradiation cabinet. A xenon lamp A15010, a High-pressure Hg lamp 400W was used as a light source. The standard distance between the UV sources and the reaction vessel is about 5 -15cm. Before starting the reaction, the reaction concoction was stirred using a magnetic stirrer in the dark room for 30 min to attain adsorption-desorption equilibrium. Under normal conditions, the reaction mixture was

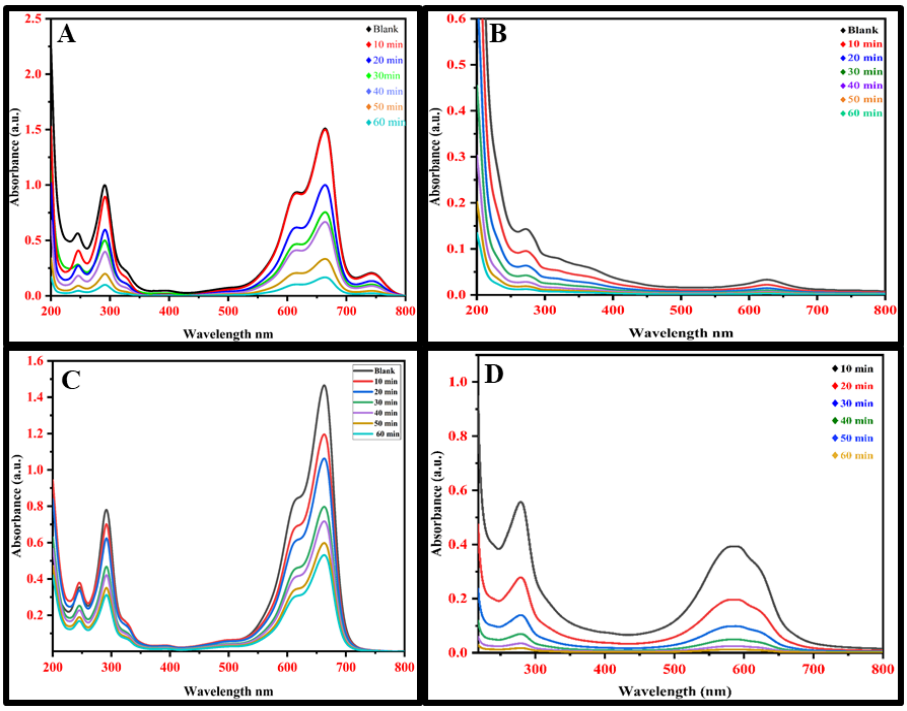

Fig. 14:(A) Uv – visible spectrum of photocatalytic degradation Of Methylene blue in an acidic medium(B)Uv – visible spectrum of photocatalytic degradation of methylene blue in basic medium(C)Uv –Visible spectrum of photocatalytic degradation of Methylene blue in neutral medium(D) Uv-visible spectrum of photocatalytic degradation of methylene blue on UV irradiation in a basic medium.

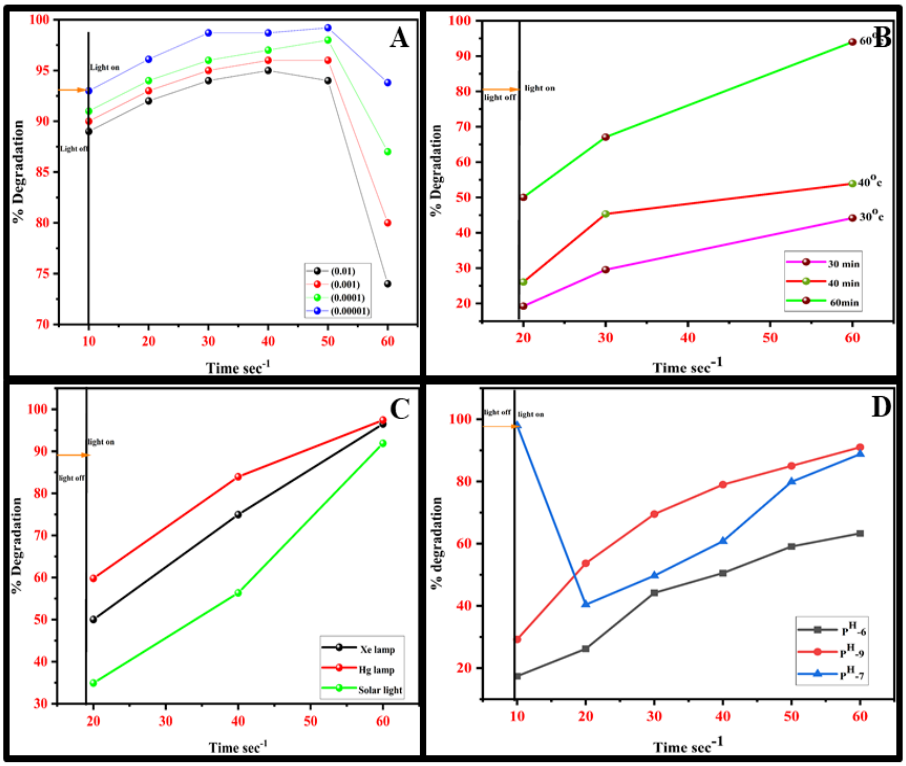

Fig. 14 (B):(i)Effect of initial concentration on the photodegradation of MB (ii) Effect of temperature on the photodegradation of MB (iii)Effect of light sources on the photodegradation of MB (iv) Effect of PH on the photodegradation of MB.

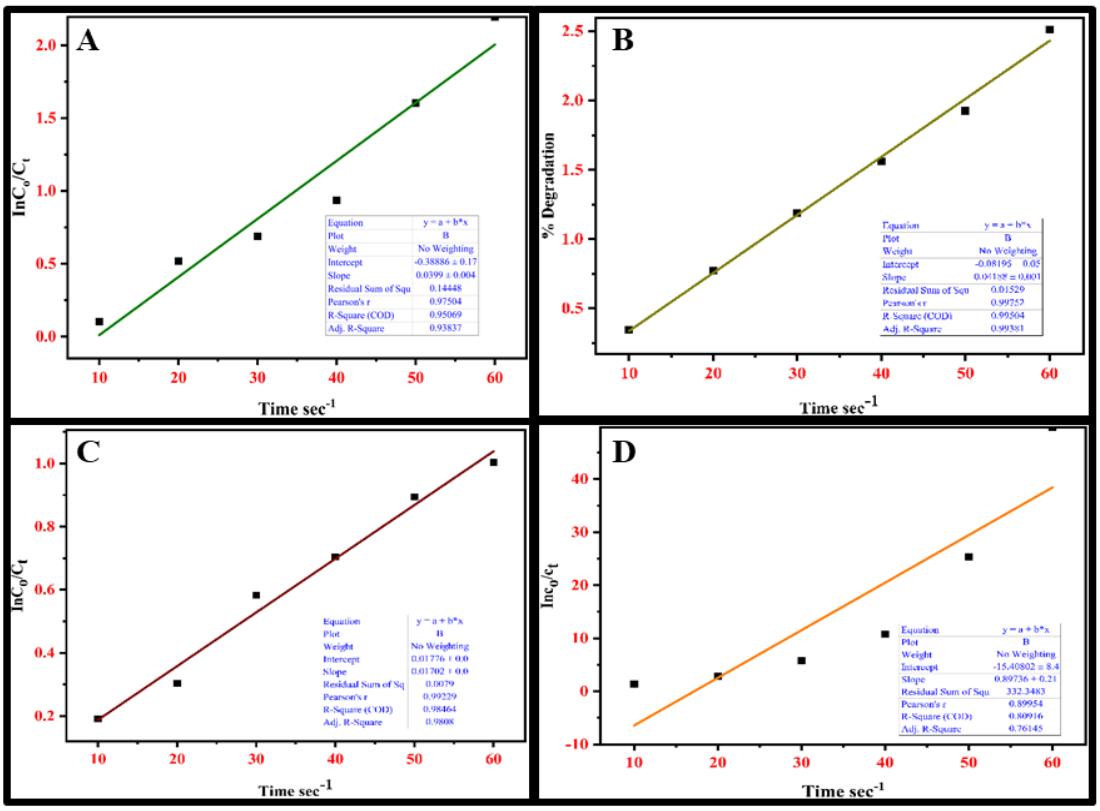

Fig. 14 (C): A linear calibration curve of InCo/Ct versus time with correlation coefficient R2 for MB dye on photodegradation

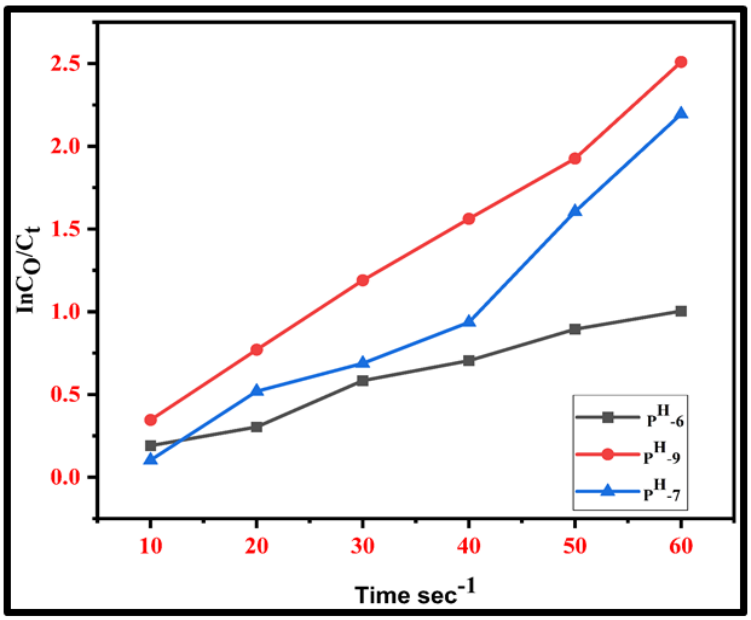

Fig. 14 (D): First-order kinetics of the degradation of MB dye under solar irradiation with SeZr BNPs in three different mediums (Catalyst dose – 0.002mg/L, dye concentration – 0.0002mg/L)

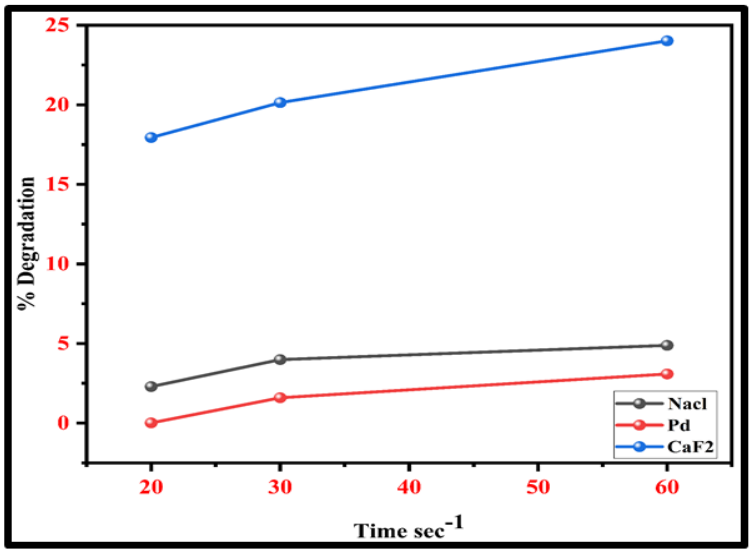

Fig. 15(A): Effect of inorganic ions on the photodegradation of MB

a

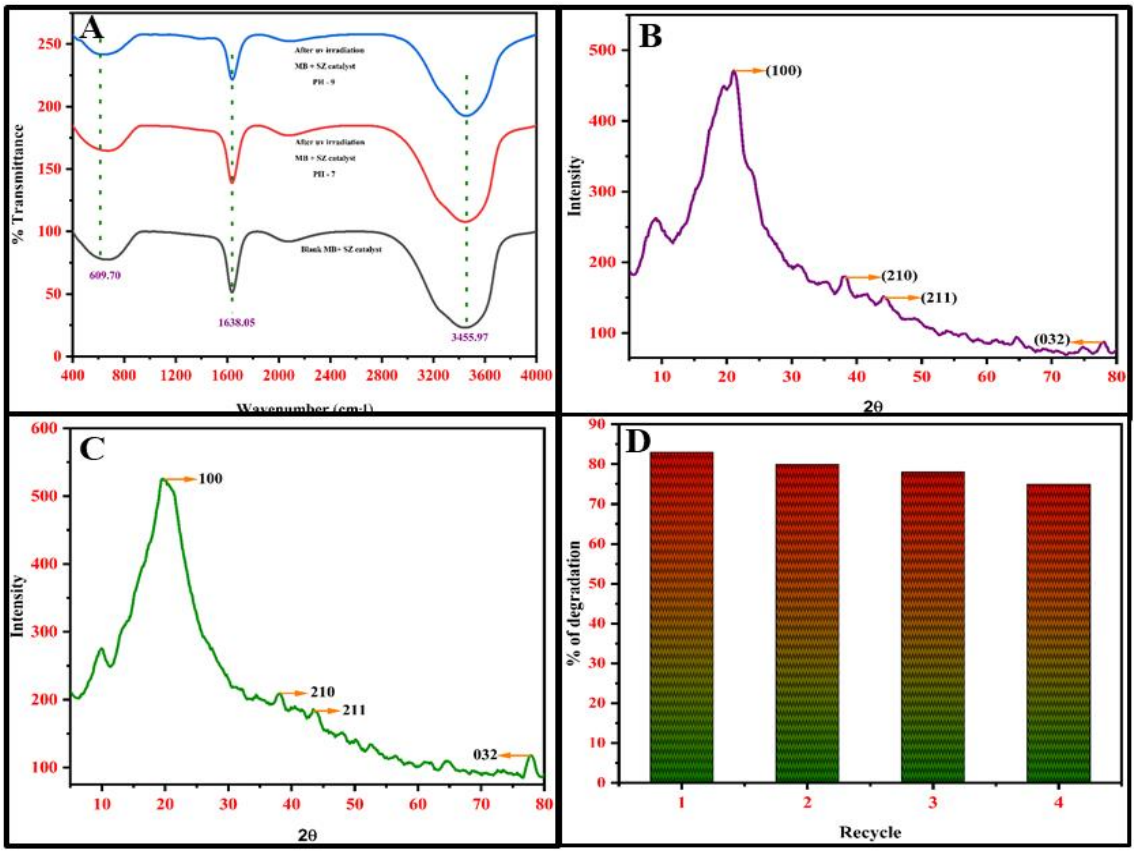

Fig. 15 (B):(A)XRD spectrum of SeZr BNPs after 4 cycles of solar irradiation(B) FTIR spectrum of photocatalyst(SeNPs) before and after solar irradiation (D)illustrate the percentage of reusability after a 5cycle turn.

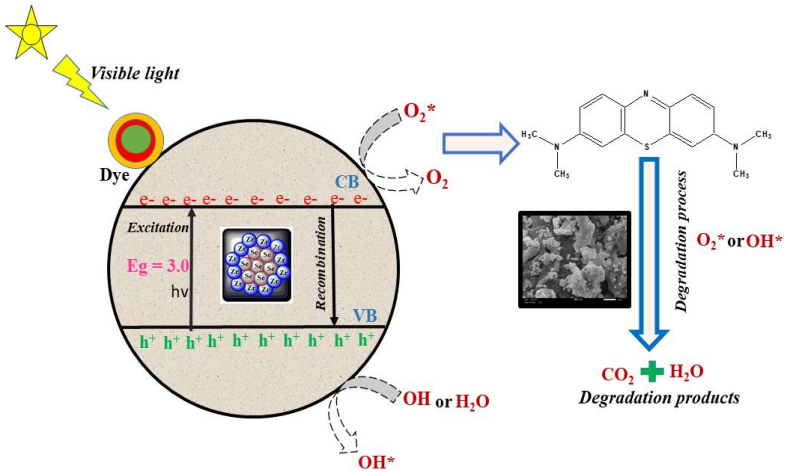

Fig. 15 (C): The photocatalytic degradation of methylene blue with bioactive SeZr BNPs under visible light irradiation

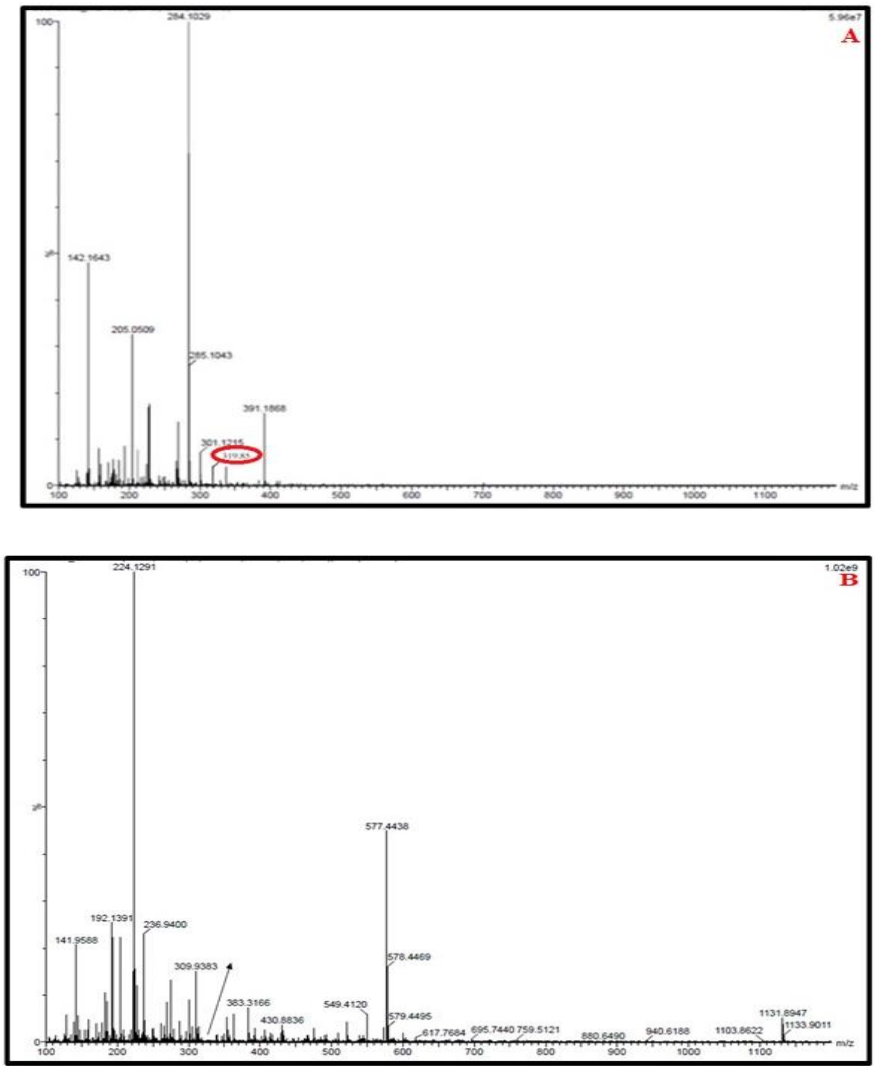

Fig. 15 (D): (A) Mass spectrum of methylene blue dye before degradation (B) Mass spectrum of degradation product after light irradiation.

Table 4. Docking score of Eugenol, Cinnamaldehyde with cancer cell lines (PDI CODE:40ar)

S.No	Compound Name	Docking score
1	Cinnamaldehyde	-5.4
2	Eugenol	-6.1

exposed to a UV – cabinet under normal conditions. [**39**]The degradation percentage was calculated using the following equation %D =Co-Ct/Co X100Co - the initial concentration of dye Ct – dye concentration after dye degradationFurther, the concentration of MB was measured with Brucker (UV – Spectrophotometer). Hence the degradation efficiency of SeZr BNps is 85% because of its small size (80nm) and the synergistic effect of the photocatalyst being observed. On the other hand, The mechanism of photocatalytic degradation of MB towards SeZr is illustrated below.

Effect of concentration of MB dye degradation

In this experiment, the effect of MB dye concentration of 0.02 – 0.00002mol/L was examined under room temperature at an optimized PH, with a catalyst dosage of 0.002g/L respectively. Fig. 1, illustrates the removal efficiency of MB at different concentration ranges. the result of this study reveals that increases in the concentration of MB dye solution will lead to decreases in photocatalytic efficiency from 85% -75% obtained based on Lambert's law. However, the photocatalytic degradation of MB was increased with decreases in concentration due to the availability of active sites at the surface of the photocatalyst.in addition, a high concentration of dye molecules on the photocatalyst will hinder the penetration of incident light within limited time lapses. Hence the increases in several occupancies of substrate ions in interlayer spacing led to the deactivation of the photocatalyst. Therefore, the photodegradation was carried out at a low concentration at room temperature, catalyst loading 0.002g/L at a high pH of 9 (Table 4 & 5) [10].

Effect of different light sources on degradation

In this analysis, the effect of some different light sources such as the Xe Lamp, the Hg lamp, and solar visible light, on photocatalytic activities were examined and compared. the degradation efficiency of photocatalysts on visible light irradiation provides more than 87% of degradation within 180 minutes, where less than 62.32% were attained with Xelamp, and Hg Lamp within 180 min under the same experimental condition. whereases, photodegradation of MB dye was increased with increases in light intensity. therefore, a high-pressure Hg lamp was selected as the best light source for degradation within a particular time. Hence, the extent of degradation above the limit of unlimited time will bring the photocatalytic system into effect due to electron-hole recombination.[**9**]

Effect of temperature on MB dye degradation

The degradation efficiency of MB solution at different temperatures (45,65,100) under optimum conditions (MB dye solution of 0.0002g/L, catalyst dosage of 0.002g/L using bioactive Sezr BNps after solar irradiation) was investigated. Fig. 1 The visible spectrum of bioactive sezr BNps at different temperature ranges. the result of the analysis shows decreases in absorbance of MB solution with increases in temperature suggesting SeZr BNps is a suitable material for photocatalytic activities at a high-temperature range [**9**].

Effect of pH On MB dye degradation

pH is one of the important parameters that can influence the degradation efficiency of the photocatalyst. The efficiency of the photocatalyst was examined by utilizing a series of solutions of MB at three different pH ranges (6,7,9) containing a catalyst dosage of 0.002g/L with a visible light intensity of 115MW/cm^2. Fig. 15 illustrates the UV–visible spectrum of MB at three different pH. The subsurface of camphora- mediated Sezr BNps has a positive charge at low pH and negatively charged at higher pH 9, respectively, in a strongly acidic medium, the protonated MB was strongly repelled by a surface catalyst, leading to decline degradation.on the other hand, an excessive amount of OCl- radical formation can occur by the reaction of cl- from acid with an OH ion, which will reduce the degradation similar to the reported literature [9,11]. In a strongly alkaline medium, the free e-pair of a nitrogen atom in MB molecules can exhibit a strong electrostatic attraction with a positively charged photocatalyst to enhance the degradation efficiency of MB dye. Therefore, the decrease in degradation efficiency is due to the low production

of hydroxyl radicals with less light penetration in an alkaline medium due to the formation of insoluble compounds with less oxidation potential. The result of this study reveals greater than 87% degradation towards MB at pH 9 under visible light radiation. However, the desorption of MB dye at the surface of the photocatalyst is too low for the moderate surface area of Sezr BNps. Hence, the effective degradation of MB at high pH is due to the formation of a large number of hydroxyl radicals in an alkaline medium.

Kinetics of photodegradation of MB dye

In the kinetic study, the photocatalytic mechanism of MB on degradation was investigated. In this analysis, optimum experimental conditions, including 0.00002mg/L of MB solution, 0.0002mg/L catalyst loading, and irradiation within 180 min at pH 9 were taken into consideration. Fig. 15 shows that the rate of the photodegradation process InC_O/C_t varied linearly concerning different time intervals, suggesting that the reaction will follow pseudo-first-order kinetics. Table 1 shows the value of R2 with K at different concentration ranges. The outcome of this analysis shows that increases in the concentration of dye from 0.00002mg/L to 0.02g/L will decrease the rate of reaction from 0.03 -0.07, respectively, with a correlation coefficient of R2= 0.9, suggesting that the reaction will follow pseudo-first-order kinetics. pseudo-first-order kinetics was used to study the rate of reaction using this formula. InCo/Ct =-KtWhere C0 is the concentration of dye at the initial time D is the dye concentration after a time interval, k – rate constant.[18]

Selectivity analysis of BNps or effect of inorganic anions

To identify the reactivity of responsible species involved in the photodegradation of MB dye solution. Some of the tests were performed with inorganic anions such as Nacl and Pd respectively. The result of this analysis shows that the presence of Na+, Cl-, and Pd ions will slow down the degradation kinetics. therefore, the presence of inorganic ions will diminish the production of O_2, leading to decreases in the degradation rate. The photodegradation efficiency of the MB solution was decreased from 85 – 75 after 40 min furthermore, other experiments were performed in the presence of CaF_2 to scavenge holes and OH – radicals. The result of this analysis shows no significant decreases in photodegradation for CaF_2 suggesting that

Table 5. Comparison of various parameters such as concentration, PH, Catalyst dosage, and rate of MB dye degradation with the previously reported studies

S.NO	Nanocatalyst	Dye	PH	Light source	Catalyst dose	Time duration	Concentration Of dye	rate	Of degradation	Reference
1.	CuO/Bi2O3	MB	3	-	0.2g/l	-	20mg/L	-	88.32	[8]
2.	WZnO/HPA	MB	-	Visible light	-	90min			>40min	[9]
3.	AgZno	MB	-	Visible light	-	-	-		ZnO – 63% AgZnO -98%	[10]
3.	MgZnO@SiO2- tetrazine	MB Ciprofloxacin	9	Visible light mercury lamp9green LED)	0.02g	3.5mg/L-1	-	0.068min-1	-	[11]
4.	Fe3O4@SnO2/Ag-rGH	2,4 DCP	-	-	-	120min	-		93.8	[14]
5	Bi/SnO2/TiO2 graphene Nanocomposite	pentachlorophenol	-	Solar visible light	-	-	-	0.007 -0.0149 min-1	84%	[15]
6	Ag-CuFe2O4@WO3	Gemfibrozil Tamoxifen	5	Uv light	0.2g/L	150min	5mg/L		81% GEM 83% TAM	[18]
8	Camphora – mediated Sezr BNps	MB	9	Visible light illumination	0.001g/L	60min	0.0001g/L		85%	Current work

Camphora mediated Sezr BNPs are some suitable materials for water purification.[18]

Stability and reusability of photocatalyst

Stability and reusability analysis of a photocatalyst is economically important to overcome the issue that arises due to the operation cost of the catalytic process. Therefore, the reusability of camphora-mediated bioactive sezr BNps for visible light-induced photodegradation of MB was examined under optimum environmental conditions for up to four successive cycles. A utilized photocatalyst was separated from the solution after numerous times washing with deionized water, and ethanol and dried by using an air direr for further degradation. A maximum percentage of degradation was attained after four cycle turns, as shown in Fig. 15. Under visible light radiation, the maximum percentage of degradation was reduced from 85 -75%. the reason for the loss of efficiency is due to the occupancy of active sites, partial aggregation of nanoparticles, and decreases in the mass percentage of photocatalysts, which lead to low MB degradation efficiency similar to that reported in the literature. Further, FTIR and XRD analysis of BNps before and after irradiation confirms the stability of the photocatalyst. [9,15]

Mechanism of photodegradation of MB blue dye

The mechanism involved in the photocatalytic degradation of methylene blue with bioactive SeZr BNPs under visible light irradiation is demonstrated in Fig. 1 As in the present studies, the Interlinking of Se with Zr nanoparticle causes e- and hole recombination and hinders charge separation. it involves the promotion of an electron from the valence band to the conduction band of the semiconductor nanoparticles, which can lead to the generation of electron–hole pairs. Further, the photogenerated holes will directly oxidize dye to reactive intermediates or with hydroxyl ions, leading to the formation of highly oxidative hydroxyl radicals (OH*), and e- in the conduction band can move towards the surface of the photocatalyst to react with O_2 species, leading to the generation of a large amount of O_2* superoxide anion free radicals, which lead to the degradation of MB on the surface of photocatalyst and can cause the complete mineralization of dye. However, in this mechanism, the hydroxyl radical is a powerful oxidizing agent. It can attack organic pollutants adsorbed at the surface of the photocatalyst, leading to a photo-oxidation reaction that can cause the degradation of MB.[8]

Mass spectrum of methylene blue on before and after degradation

The ESI – MS spectrum of the methylene blue and the degradation product was performed to determine the molecular weight and fragmentation. The molecular ion peak observed at m/z 319.0 assigned (M+H) peak of methylene blue are shown in Fig. 1. whereases the disappearance of the peak in the region at m/z 284 conforms to the degradation products of methylene blue as per the reported literature [55].

Docking Activities of some of the components in camphora products with breast cancer cell lines

Molecular docking activities were performed using Auto DOCK tools 1:5:6 on compounds 1 and 2 (Eugenol, Cinnamaldehyde). Interaction of ligand (Eugenol, Cinnamaldehyde) on the acceptor site of 40ar reveals electrostatic interaction on residue THR(A:829), SER(A:757), HIS(A:81) sites, and covalent bond interaction occurs at O-H sites revealing the anticancer result of the eugenol compound. In addition, a weak Vander wall's interaction occurs at the binding sites of 40ar on residue TYR(A:953), VAL(A:925), Lys(A:919), PRO(A:918), HIS (A:888), VAL (A:884). The binding affinity of Eugenol and cinnamaldehyde is -6.1 and -5.4 respectively, which are greater than the inhibitory activity of eugenol with the IYVB chain (-4.8—5.3) and similar to the binding of COX -2(-6.69 with cyclooxygenase, peroxidase active site), and (-6.59 – 6.02 for 5 -LOX with heme pocket, hydrophobic pocket on eugenol [**56**] Hence, the high negative value of Eugenol compared to cinnamaldehyde shows the stability of the compound in binding to the receptor site. Whereases, in the event of cinnamaldehyde Strong electrostatic interaction of ligand on binding sites of amino acids residue such as PhE (A:778), ILE(A:699), ARG (A:766), and GLN(A:725) at the O –H position and weak interaction exhibit at LEUA:721, ALA9A:779), PRO(A;696), VAL(A:729), Lys(A:822), and SER(A:728) reveals the binding affinity of the compound with cancer protein.

CONCLUSION

In the current work, *Cinnamomum camphora*-mediated SeZr BNPs were biosynthesized to

remove the aqueous solution of methylene blue dye. The effect of parameters such as PH, concentration of dye solution, and temperature under solar irradiation was studied. The degradation efficiency of SeZr BNPs is tested at three different P^H 6,7,9. The result of this study shows higher degradation efficiency and rate in the alkaline medium due to excessive OH^- radicals than in the acidic medium. Hence, the percentage of degradation methylene blue (97%) in the basic medium conforms to the catalytic activity of BNPs. Moreover, optical band gap measurement was performed at room temperature, and the band gap energies of Se and SeZr photocatalyst were 2.5 and 3.0 respectively. The rate of photocatalytic reaction was calculated to be 0.003 min-1 with a linear correlation coefficient R_2 -= 0.9, suggesting that the reaction follows pseudo-first-order kinetics. The photocatalyst exhibits good stability after 4 cycles of reuse. Further, the selectivity analysis confirms the activity of BNPs toward MB deterioration. Finally, the cytotoxic activities of *camphora*-mediated SeZr BNPs were exhibited at a MIC of 38.9µg/ml, which was less than that of TeCe but greater than that of TeSe, TeZr conforms to the anticancer effect and biocompatibility of BNPs. In addition, docking activities will theoretically conform the binding affinity of components (Eugenol, cinnamaldehyde) with cancer protein.

CONFLICT OF INTEREST

The authors hereby declare that there is no conflict of interest.

REFERENCES

1. W.W. Anku, S.O.oppong, S.k.Shukla, and p.p.govender, Comparative photocatalytic degradation of monoazo and diazo dyes under stimulated visible light using Fe+3/C/S doped TiO2 nanoparticles, Scientific paper, 63 (2016) 380 -391, https://doi.org/10.17344/acsi.2016.2385
2. E. Fosso - kankeu, F. waanders, and M. Geldenhuys, Photocatalytic degradation of dyes using TiO2 nanoparticles of different shapes, international conference on latest trends in engineerin & technology, (2015)1-7.
3. Sonde,O.I,Oloyede,A.R.Oladoyinbo,F.O.Sanyaolu,N.O.Ibikunle,A.A,Afolabi,T.A.Aro -tiba,O.A.Dare,E.O,synthesis and characterization of Se-ZnO photocatalyst with improved photodegradation and antibacterial properties.5(1) (2018)30-34.https://doi.org/10.154361.2377-1372.18.1796
4. S.Moosavi, R.Y.M. Li, C. W. Lai, Y. Yusof, S.G.O.A. Zadeh, Z.Z.C.X. Yue, and M.R.B. Johan, Methylene blue dye photocatalytic degradation over synthesized Fe3O4/AC/TiO2 nanocatalyst: degradation and reusability studies,Nanomaterials,10(12):2360(2020)1-16, https://doi.org/10.3390/nano10122360
5. Z.Z.Vasiljevic,M.P.Dojcinovic,J.D.V.Ceric,I.Jankovic-castvan,M.ognjanovic,N.B Tadic,S.Stojadinovic, G.O.Brankovic and M.V.Nikolic, photocatalytic degradation of methylene blue under natural sunlight using iron titanate nanoparticles prepared by a modified sol-gelmethod. Royalsocietyopenscience7:200708(2020)1-14. https://doi.org/10.1098/rsos.200708
6. M.A.Abu - Dalo, S.A.Al -Rosan and B.A.Albiss, Photocatalytic degradation of methylene blue using polymeric membranes based on cellulose Acetate impregnated with Zno nanostructures,polymers,13(19):3451 (2021)1-18. https://doi.org/10.3390/polym13193451
7. A. Fouda, S.E. Hassan, A. M.Eid, M. A. Abdel - Rahman & M. F.Hamza, Light enhanced the antimicrobial, anticancer, and catalytic activities of selenium nanoparticles fabricated by endophytic fungal strain, Pencillium crustosum Ep -1,Scientific reports,12:11834 (2022)1-16. https://doi.org/10.1038/s41598-022-15903-2
8. F.poorsajadi, M.H. sayadi, M.Hajiani and M.R. Rezaei,Synthesis of CuO/BiO3 nanocomposite for efficient and recycling photodegradation of methylene blue dye,international Journal of Environmental analytical chemistry,(2020) https://doi.org/10.1080/03067319.2020.1826464
9. R.Tayebee,E.Esmaeili,B.maleki,A.Khoshniat,M.chahkandi,N. Mollania,photodegradation of Methylene blue and some emerging pharmaceutical micropollutants with an aqueous suspension of WZnO-NH2@H3PW12040 nanocomposite,Journal of molecular liquids,317(2020)113928,1-13. https://doi.org/10.1016/j.molliq.2020.113928
10. R.M Kakhki,R.Tayebee,F. Ahsani,New and highly efficient Ag doped ZnO visible nano photocatalyst for removing of methylene blue,J.Mater.sci.mater electron,(2017)1-12. https://doi.org/10.1007/s10854-016-6268-5
11. E.Parvizi,R.Tayebee,E. Koushki,M. F.Abdizadeh,B.Maleki,P. Audebert and L.Galmiche,Photocatalytic efficiency of supported tetrazine on MgZnO nanoparticles for the heterogenous photodegradation of methylene blue ciprofloxacin,Rsc Adv,9(23818) (2019)1-14. https://doi.org/10.1039/C9RA04702F
12. L.Shruthi, shyni,K.Jagadish,Dr.S.Srikantaswamy,M.R.Abhilash,Photocatalytic degradation and removal of heavy metals in pharmaceutical waste by selenium doped ZnOnanocomposite semiconductor2 (2016)1-9,journal of research.
13. C.Zhao,Z. Liu,Y.Wu,J.Guo,P.Huang,Y.Wang,Y.Leng,I.P.Pozdnyakov,J.Xu,F. Wu,EDTA enhances the photodegradation of P-Arsanilic acid in the presence of iron at near neutral PH,ChemicalEngineeringJournal,450:137984(2022)1-16. https://doi.org/10.1016/j.cej.2022.137984
14. A.Rezaei,M.R.rezaei,MH. sayadi,3D network structure graphene hydrogel - Fe3O4@SnO2/Ag via an adsorption /photocatalysis synergy for removal of 2,4 dichlorophenol.journal of the Taiwaninstitute of chemical engineers,121(2021)154-167. https://doi.org/10.1016/j.jtice.2021.03.048
15. M.H.sayadi,S.H.A.Rezaei, H.Shekari,Bi/SnO2/TiO2 graphene nanocomposite photocatalyst for solar visible light - induced photodegradation of pentachlorophenol, Environmental science and pollution research (2020) https://doi.org/10.1007/s11356-020-11708-w
16. B. Li,R. Tayebee,E. Esmaeili,M. S.Namaghi and B.maleki,Selective photocatalytic oxidation of aromatic alcohols to aldehyde with air by magnetic WO3ZnO/Fe3O4 insitu photochemical synthesis of 2- substituted benzimidazoles,Rsc

Adv,10(40725) (2020) 1-14. https://doi.org/10.1039/D0RA08403D
17. R.Chen,Z.Jalili and R. Tayebee,Uv- visible light induced photochemical synthesisof benziimidazoles by coomassie brillent blue coated on W-ZnO@NH2 nanoparticles,Rsc Adv, 11(16359)(2021)1-17. https://doi.org/10.1039/D0RA10843J
18. M.H.sayadi,N.AhmadpourandS.Homaeigohar,Photocatalyticandantibacterialpropertiesof AgCuFe2O4@WO3magnetic nanocomposite,nanomaterials,11(2021)1-19. https://doi.org/10.3390/nano11020298
19. T.Li,H. Xu,Selenium - containing nanomaterials for cancer treatment, Cell reports physical science,1(2020)1-17. https://doi.org/10.1016/j.xcrp.2020.100111
20. R.M.A.Abdelaleem,H. F. A. Hameed,M. E. Askar, S. Hassan,M. Hassan and A. I. El - Batal,Modulatory role of selenium nanoparticles and grape seed extracts mixture on oxidation stress biomarkers in diabetics irradiated rats, Indian Journal of pharmaceutical education and Research.50 (2016) 170-178. https://doi.org/10.5530/ijper.50.1.21
21. P. Sonkusre and S.S. cameotra, Biogenic selenium nanoparticles induce ROS - Mediated necroptosis in PC -3 cancer cells through TNF activation,Journal of Nanobiotechnology,15:43 (2017)1-12. https://doi.org/10.1186/s12951-017-0276-3
22. R Hassanien, A.A.I. Abed -Elmageed and D.Z.Husein, Eco-friendly approach to synthesize selenium nanoparticles: photocatalytic degradation of sunset yellow Azo Dye and Anticancer activity,Materials science inc.Nanomaterials & polymers,4 (2019) 9018 -9026. https://doi.org/10.1002/slct.201901267
23. M.Nagalingam,S.R. Kumar,S. K. Balu, M.Tharani and K. Arunachalam,Anticancer and antioxidant activity of Morinda Citrifolia leaf mediated selenium nanoparticles Journalofnanomaterials,Article:2155772 (2022)1-7. https://doi.org/10.1155/2022/2155772
24. G. Liao,J. Tang,D. Wang,H. Zuo,Q. Zhang,Y. Liu, and H. Xiong,Selenium nanoparticles (SeNps) have potent antitumor activity against prostate cancer cells through the upregulation of miR-16,WorldJournalofsurgical oncology18:81(2020)1-11. https://doi.org/10.1186/s12957-020-01850-7
25. S.A.Wadhwani, M.Gorain, P.Banerjee,U.U. balkar, R.Singh, G. C Kundu, and B.A chopade, Green synthesis of selenium nanoparticles using Acinetobacter Sp.SW30: optimization,characterization and its anticancer activity in breast cancercells,InternationalJournalofNanomedicine,12(2017)6841- 6855. https://doi.org/10.2147/IJN.S139212
26. O.Bilek,Z.Fohlerova, and J.Hubalek,Enhanced antibacterial and anticancer properties of SeNps decorated TiO2 nanotube flim,plos one,14(3):e0214066 (2019)1-15. https://doi.org/10.1371/journal.pone.0214066
27. C.H.Ramamurthy,K.S.Sampath,P.Arunkumar,M.S.Kumar,V. Sujatha,K.premkumar,C.Thirunavukkarasu, Green synthesis, and characterization of selenium nanoparticles and its augmented cytotoxicity with doxorubicin on cancer cells, Bioprocess Biosyst Engineering, 36(8)(2013)1131 -1139. https://doi.org/10.1007/s00449-012-0867-1
28. G. Liao,J. Tang,Diwang,H. Zuo,Q. Zhang,Y. Liu,and H, Xiong,Selenium nanoparticles (SeNps) have potent antitumor activity against prostate cancer cells through the upregulation of miR-16,word journal of surgical oncology,18:81(2020)1-11. https://doi.org/10.1186/s12957-020-01850-7
29. K.Spyridopoulou,G.Aindelis,A.pappa,K.chlichlia,Anticancer activity of biogenic selenium nanoparticles:Apoptotic and immunogenic cell death markers in colon cancer cells,13 (2021)1-22. https://doi.org/10.3390/cancers13215335
30. M.Vahdati & T.T. Moghadam,Synthesis and characterization of selenium nanoparticles - Lysozyme nanohybrid system with synergistic antibacterial properties,Scientific reports, 10:510 (2020)1-10. https://doi.org/10.1038/s41598-019-57333-7
31. S.Balaji,B.K. Mandal,S. Ranjan, N. Dasgupta,R. Chidambaram,Nano zirconia - evaluation of its antioxidant and anticancer activity,Journal of photochemistry & photobiology,(2017)1-41. https://doi.org/10.1016/j.jphotobiol.2017.04.004
32. V. Bartunek ,B. Vokata,K. Kolarova,P. ulbrich,Preparation of amorphous nano - selenium - PEG composite network with selective antimicrobialactivity,materialsLetters,238(2019)51-53. https://doi.org/10.1016/j.matlet.2018.11.134
33. J.vyas and S. Rana, Biosynthesis of selenium nanoparticles using Aloe vera leaf extract, , InternationalJournalofAdvancedresearch,6(1)(2018)104-110, https://doi.org/10.21474/IJAR01/6191
34. Chrys O.Chikere,Nadimul Haque faisal,Paul Kong -Thoo -Lin and carlos Fernandez, Interaction between Amorphous zirconia nanoparticles and graphite : electrochemical application for gallic acid sensing using carbon paste electrodes in wine,nanomaterials,10: 537 (2020)1-25. https://doi.org/10.3390/nano10030537
35. K. Kalishwaralal,S.C.B. Jeyabharathi, K. Sundar& A.M. Kumaran, Anovel one - spot green synthesis of selenium nanoparticles and evaluation of its toxicity in zebrafish embryos, Nanomedicine and Biotechnology,44:2(2014)471-477. https://doi.org/10.3109/21691401.2014.962744
36. Sareh Bagheri - Josheghani and Bita Bakhshi, Investigation of the antibacterial and antibioflim activity of selenium nanoparticle against Vibro cholerae as a potent therapeutics,Article ID :3432235 (2022) 1-10. https://doi.org/10.1155/2022/3432235
37. C.wang,Q. Hu,Y.wei,D.Fang,W. Xu,Z. Luo,Facile fabrication of selenium (Se) nanowires for enhanced lithium storage in Li -Se battery,Ionics,(2017)1-9. https://doi.org/10.1007/s11581-017-2164-0
38. S.R.Teeparthi,E.W. Awin & Ravikumar,Dominating role of crystal structure over defect chemistry in black and white zirconia on visible light photo catalytic activity, Scientific reports 8:5541 (2018)1-12. https://doi.org/10.1038/s41598-018-23648-0
39. S.S.Salem,M.S.E.MBadawy,A.A.Al-Askar,A.A.Arishi,F.M.ElkadyandA. H.Hashem,Green biosynthesis of selenium nanoparticles using orange peel waste : characterization,Antibacterial and antibioflim activities against multi drug - resistant bacteria12 (2022)1-12. https://doi.org/10.3390/life12060893
40. F.yang,J. Huang,H. X. Liu,W. Lin,X. Li,X. Zhu,T. chen,Lentinan -functionalized selenium nanosystems with high permeability unfiltrate solid tumour by enhancing transcellular transport, nanoscale (2020)1-11. https://doi.org/10.1039/D0NR02171G

41. D.M. Cruz, W. Tien Street, B. Zhang, X. Huang, A.V. Crua, A. Nieto-Arguello, J.L. Cholula Diaz, L. Martinez, Y.H.Maria, U. Gonzalez, J.M. Garcia-Martin, T. J. Webster, Citric juice - mediated synthesis of tellurium nanoparticles with antimicrobial and anticancer properties, Green. Chem, (2019) 1-50.
42. R. Hosseinzadeh & K. Khorsandi,photodynamic effect of zirconium phosphate biocompatible nano-bilayers contaioning methylene blue on cancer and normal cells,scientific reports,9:14899(2011) https://doi.org/10.1038/s41598-019-51359-7
43. M.sridharan,P.kamaraj,Vennilaraj,J.Arockiaselvi,T.Pushpamalini,P.A.Vivekanand,S.Harikumar,Synthesis,characterization and evaluation of biosynthesized cerium oxide nanoparticle for its anticancer activity on breast cancer cell(MCF),Materials Today : Proceeding,(2020)2214 -7853. https://doi.org/10.1016/j.matpr.2020.07.031
44. S. A. Nezhad, A.Eshaghi, M. H. Tabrizi, Green synthesis of cerium oxide nanoparticle using Origanum Majorana L.leaf extract, its characterization, and biological activities, Applied organometallic chemistry, e5314 (2019)1-10. https://doi.org/10.1002/aoc.5314
45. R.Anitha, K.V Ramesh, K.H.S. Kumar, Synthesis, characterization of Ceo2 nanoparticles via eco-friendly green combustion technique and its antimicrobial, anticancer activities, International Journal of advanced science and technology, 28(7) (2019) 74 -96.
46. P. Nithya, M. Balaji, A. M. Krishnan, C. D. Kumari, S. Rajesh, A. Surya, M. Sundrarajan, Ionic liquid functionalized biogenic synthesis of AgAu bimetal doped CeO2 nanoparticles from Justicia adhatoda for pharmaceutical Application: Antibacterial and anticancer activities, Journalofphotochemistry&photobiologyB:biology,(2019)1-45, https://doi.org/10.1016/j.jphotobiol.2019.111706
47. M. Hosseini, I. Amjadi, M. Mohajeri, and M. Mozafari, Sol - gel synthesis,physico - chemical and biological characterization of cerium oxide/polyallylamine nanoparticles, polymers,12 (2020)1-14. https://doi.org/10.3390/polym12071444
48. S.pon,S.SriV&M.George,Spherical CeO2 nanoparticles encapsulated with Nelumbonucifera gaertn. flower extract and its in-vitro anticancer activity against HCT116 Human colon cancer cell line, Indian Journal of chemical technology, 27 (2020)153-160.
49. L.T. N. Ngoc, S. park, J. oh, Hoyunshin, M. kim, H.U. Lee, K. Lee, K. Lee, J. moon, O. Kwon, H. Y. Yang, and Y. Lee, Cerium Amino clay - a Potential hybrid biomaterial for anticancer therapy, ACS Bio materials Science&.Engineering, 5 (2019)5857 -5871. https://doi.org/10.1021/acsbiomaterials.9b00789
50. M.S.vidhya, F.Ameen, T.Dawoud, R.Y. Kumar, G.Ravi, P. Kumar, D. Velauthapillai, Anti-cancer applications of Zr, Co, Ni-doped Zno thin nanoplates,283:128760 (2021)1-4. https://doi.org/10.1016/j.matlet.2020.128760
51. J.saffari -chaleshtori, E. Heidarian, S.M shafiee, Apoptotic effects of bilirubin on skin cancer cell lines SK - MEL -3 (melanoma) and A431 (non-melanoma), 21(4) (2021) 1871 -1882. https://doi.org/10.2174/1871520621999201208201134
52. S.Nazir, M.Umar,A. Khan,W.S.Al -Arjan, S.IA.Razak, A. Javed, M.R.A. Kadir, Nanocomposite hydrogels for melanoma skin cancer care and treatment: In - vitro drug delivery, drug releases kinetics and anti-canceractivities,ArabianJournalofchemistry, 14(2021)1-33. https://doi.org/10.1016/j.arabjc.2021.103120
53. X.C. wang, Z. wang, W. Ma, X. Wu, W. Fang, C. H. Guo, Y.X. Jin, Construction of a nonotheranostic system Zr- MOF@ppa/AF@PEG for improved photodynamic therapy effects based on the PDT - oxygen consumption and hypoxia sensitive chemotherapeutic drug, Journal ofphotochemistry&-PhotobiologyB:Biology,222:112274(2021)1-11. https://doi.org/10.1016/j.jphotobiol.2021.112274
54. A.S.vig,A.gupta, O.P.Pandey, efficient photodegradation of methylene blue(MB) under solar radiation by ZrC nanoparticles, Advanced powder technology (2018) 1-12. https://doi.org/10.1016/j.apt.2018.06.007
55. L.ARIANIE,WIDODO,E.D.IFTITAH,WARSITU,Natural-isothiocyanate anti -malaria: Molecular docking ,Physiochemical ADME,toxicity and synthetic accessibility study of eugenol and cinnamaldehyde, International journal of Applied pharmaceutics.13(2021)82-88. https://doi.org/10.22159/ijap.2021v13i6.42292